Bioorganic Chemistry xxx (xxxx) xxxx

Contents lists available at ScienceDirect

Bioorganic Chemistry

journal homepage: www.elsevier.com/locate/bioorg

Discovery of benzo[*d*]oxazole derivatives as the potent type-I FLT3-ITD inhibitors

Jiyin Bao[a,1], Haichun Liu[b,1], Yanle Zhi[c], Wenqianzi Yang[b], Jiawei Zhang[b], Tao Lu[d], Yue Wang[a,*], Shuai Lu[b,*]

[a] School of Science, China Pharmaceutical University, Nanjing 211198, PR China
[b] Laboratory of Molecular Design and Drug Discovery, China Pharmaceutical University, Nanjing 211198, PR China
[c] School of Pharmacy, Henan University of Chinese Medicine, Zhengzhou 450046, PR China
[d] State Key Laboratory of Natural Medicines, China Pharmaceutical University, Nanjing 210009, PR China

ARTICLE INFO

Keywords:
FLT3 inhibitor
AML
Benzo[*d*]oxazole

ABSTRACT

Fms-like tyrosine kinase 3 (FLT3) has been considered as a potential drug target for the treatment of acute myeloid leukemia (AML), because of its high and aberrant expression in AML patients, especially the patients with FLT3-ITD mutation. Initiating from a hit compound (IC_{50}: 500 nM against FLT3-ITD), a series of compounds were designed and synthesized based on benzo[*d*]oxazole-2-amine scaffold to discover new potent FLT3-ITD inhibitors. During the medicinal chemistry works, flexible molecular docking was used to provide design rationale and study the binding modes of the target compounds. Through the mixed SAR exploration based on the enzymatic and cellular activities, compound **T24** was identified with potent FLT3-ITD inhibitory (IC_{50}: 0.41 nM) and anti-proliferative (IC_{50}: 0.037 μM against MV4-11 cells) activities. And the binding mode of **T24** with "DFG-in" FLT3 was simulated by a 20-ns molecular dynamics run, providing some insights into further medicinal chemistry efforts toward novel FLT3 inhibitors in AML therapy.

1. Introduction

Acute myeloid leukemia (AML) is a clonal hematopoietic disorder characterized by the excessive proliferation and block in differentiation of abnormal leukemic cells [1]. Although the so-called "7 + 3" regimen (combination of standard-dose cytarabine with daunorubicin or idarubicin) and the allogeneic stem-cell transplant are widely used in treating AML, the 5-year overall survival for younger patients is 40%-50%, and for elderly patients (> 60), the bulk of AML cases, is only 10%-20% [2]. AML is thus still among the refractory blood tumors with unmet therapeutic needs.

Fms like tyrosine kinase 3 (FLT3), a member of the class III receptor tyrosine kinase family (RTK), plays a key role in the proliferation, survival, and differentiation of hematopoietic stem cells [3]. However, mutations and aberrant expression of the FLT3 are closely related with the initiation and development of AML. Overexpression of FLT3, which is an unfavorable prognostic factor for the overall survival in AML, occurs in 70–100% of AML patients, [4]. Furthermore, activating mutations of FLT3 are present in 30% of AML patients, and are associated with the poor prognosis, too [5]. Particularly, approximately 25% of AML patients have the internal tandem duplication (ITD) mutations in the juxtamembrane region of FLT3, an indication of poor outcome and relapse of AML [6]; while point mutations in the activation loop of FLT3, which can stabilize the active conformation, have also been identified in 5% AML patients [7]. Recently, a number of small-molecule FLT3 inhibitors are reported, and some clinically advanced inhibitors show promising results for the treatment of AML [8–9], such as sorafenib [10], midostaurin [11] (marketed in 2017), crenolanib [12], quizartinib [13] (marketed in Japan in 2019), gilteritinib [14] (marketed in 2018) (Fig. 1). However, responses of AML patients to those inhibitors are transient, and the disease relapse often occurs within a few weeks. The drug resistance of FLT3 inhibitors was mainly caused by the FLT3 gene amplification, the expression of drug efflux pumps, the suboptimal pharmacokinetics and pharmacodynamics, the activation of other signal pathways and the mutations in the FLT3 binding domain [8]. For instance, the plasma concentration of midostaurin was decreased due to the hepatic drug metabolism including CYP3A4 [15]. Increased phosphorylation of AXL kinase was seen for after the treatment with FLT3 inhibitors [16]; this may be correlated with the drug resistance of gilteritinib. Mutations of residues D835 and F691 led to

* Corresponding authors.
E-mail addresses: zwy_1115@126.com (Y. Wang), lu_shuai@cpu.edu.cn (S. Lu).
[1] J.Y. Bao and H.C. Liu contributed equally.

https://doi.org/10.1016/j.bioorg.2019.103248
Received 16 May 2019; Received in revised form 29 August 2019; Accepted 3 September 2019

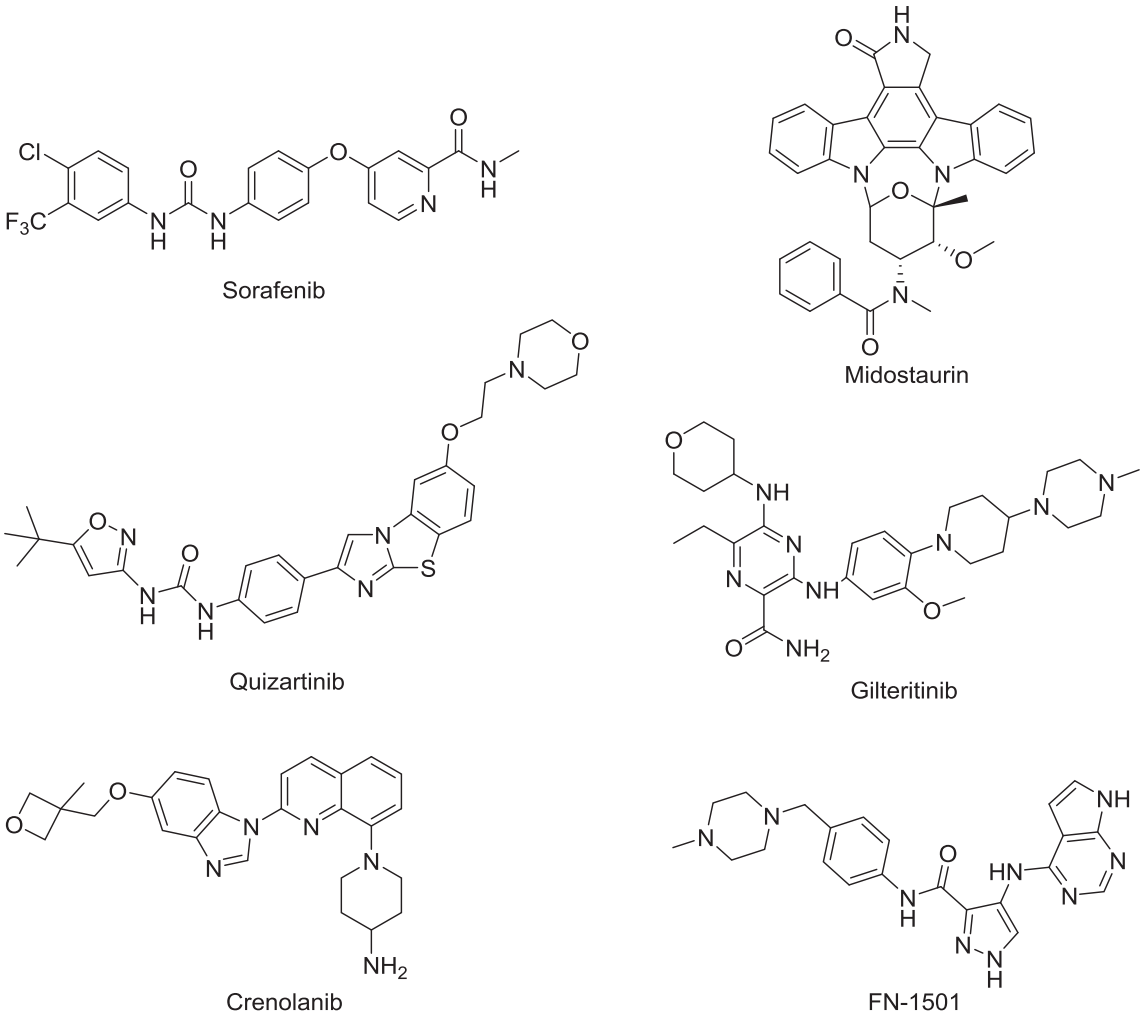

Fig. 1. Structures of the representative FLT3 inhibitors.

the acquired resistance to quizartinib [17,18]. Therefore, FLT3 is an attractive therapeutic target for treatment of AML, and new FLT3-ITD inhibitors are still urgently needed.

Previously, we reported a series of FLT3 inhibitors with the pyrazole amine scaffold [20,21], among which FN-1501 (Fig. 1) has entered phase I clinical trial [22]. To discover structurally new FLT3-ITD inhibitors, screening our in-house kinase inhibitors database was conducted, and then a hit compound **LT-793-323** (Fig. 2) was identified with moderate inhibitory activity against FLT3-ITD (IC_{50}: 500 nM). In this work, we explored the SAR of the benzoxazole compounds derived from **LT-793-323** with the assistance of structure-based molecule design method, and a new potent FLT3-ITD inhibitor with strong antiproliferative efficacy against MV4-11 cells was discovered.

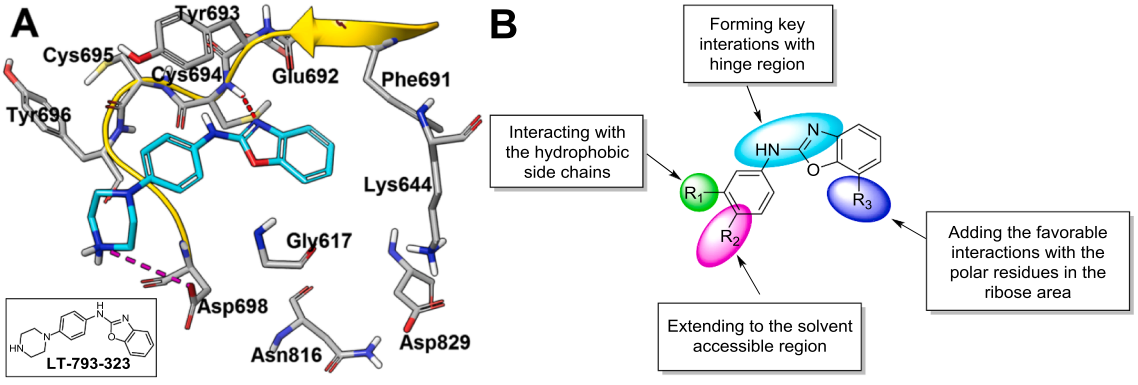

Fig. 2. (A) Flexible molecular docking-based binding mode of the hit compound **LT-793-323** with FLT3 homology model (the grey and cyan sticks represent residues of FLT3 and the hit compound, respectively; the yellow ribbon represents the hinge region; the red and purple dash lines represent the hydrogen bond and the salt bridge, respectively). (B) 2D schematic of the design rationale.

2. Results and discussion

2.1. Design rationale

In order to understand the binding mode of **LT-793-323** with FLT3, we firstly performed the molecular docking study. Since **LT-793-323** lacks the typical moieties that could bind to the allosteric pocket of "DFG-out" FLT3, we used our homology model structure of "DFG-in" FLT3 [20–22] in the docking study. As shown in Fig. 2A, the 2-amino oxazole moiety formed a hydrogen bond with Cys694 in the hinge region, the benzene linker presented in the hydrophobic area adjacent to the hinge region, and the piperazine moiety directed into the solvent accessible region, according with the canonical binding mode of type I kinase inhibitor. Normally, the hydrogen bonding interaction with the hinge region was key to the kinase inhibitors, thus the 2-amino oxazole moiety was regarded as the chemical scaffold. In comparison, addition of suitable substituents on the benzoxazole moiety might introduce some extra favorable intermolecular interactions with the unoccupied ribose binding area of FLT3 binding site. Meanwhile, adding small hydrophobic substituents onto the benzene linker might be favorable to interact with the hydrophobic side chains of its surrounding residues. The hydrophilic piperazine moiety was also worthy of investigation since it might influence the cellular potency. Therefore, we did the medicinal chemistry efforts on R_1-R_3 of the hit compound rationally to improve its enzymatic and cellular inhibitory potencies (Fig. 2B).

2.2. Chemistry

A total of 24 benzo[*d*]oxazole-2-amine derivatives were synthesized to explore the structure–activity relationships (SARs). Compounds **T1–T24** were prepared by the general approach shown in Scheme 1. The substituted *p*-fluoronitrobenzene was used as the starting material, and compounds **1a–1h** were prepared through a nucleophilic substitution reaction. Reduction of compound **1a–1h** with 80% hydrazine hydrate gave compounds **2a–2h** which were then reacted with 1,1′-thiocarbonyldiimidazole to form the isothiocyanates **3a–3h**. 2-Amino-6-bromophenol was coupled with the isothiocyanates **3a–3h**, following by the ring closure reaction to give intermediates **4a–4h**. Coupling **4a–4h** with various borate esters or boric acids yielded title compounds **T18–T21** and intermediates **5a–5t.** Title compounds **T1–T17** and **T22–T24** were subsequently obtained through deprotection of **5a–5t** by the acidic cleavage. The structures of title compounds were confirmed by the ^{1}H NMR and high-resolution mass spectra analyses (details can be found in supporting information).

2.3. Biological activity evaluation and docking study

All the synthesized compounds were evaluated for their abilities to inhibit FLT3-ITD with FN-1501 as the positive control. And the compounds that exhibited potent FLT3-ITD inhibitory activity were then measured for their antiproliferative efficacy against MV4-11 cell line, the growth of which was stimulated by the FLT3-ITD activation. The methods used in biological evaluation were provided in the supporting information. The results are summarized in Tables 1 and 2.

The first strategy for enhancing potency against FLT3-ITD was to introduce the various groups in the ribose binding area of FLT3. As shown in Table 1, the addition of the tetrahydropyridine group (**T1**) increased the FLT3-ITD inhibitory activity by almost 10 folds, suggesting that it was beneficial to incorporate new interactions with the ribose binding area. Introduction of dihydro-2*H*-pyran group yielded compound **T2** with the potent FLT3-ITD inhibitory activity (IC_{50}: 17.6 nM). However, both compounds **T1** and **T2** showed the weak cellular efficacy against MV4-11 cells. Therefore, we continued to investigate other groups. The incorporation of aromatic rings such as the benzene (**T3**), 3-pyridine (**T4**), 4-pyridine (**T5**) or pyrazole (**T6**), all improved the FLT3-ITD inhibitory activities by about 10 folds (IC_{50}: 38.52, 21.22, 30.41 and 57.04 nM, respectively) as compared with compound LT-793-323, but still showed the weak cellular activities.

Considering that the ribose binding area was surrounded by the polar side chains of FLT3 residues, including Lys644, Asp698, Asn816 and Asp829, we assumed that the polar interactions with those side chains would be beneficial to increase the kinase inhibitory activity. As expected, the addition of *meta*-amino (**T7**), *meta*-methoxy (**T8**), *meta*-cyano (**T9**) group or *meta*-chlorine (**T10**) on the phenyl ring all made obvious increase in the enzymatic activity, among which **T9** displayed the potent kinase activity (IC_{50}: 1.02 nM) and **T8** showed the potent cellular efficacy (IC_{50}: 0.41 μM), respectively. Docking study showed that the amino group of **T7** and the cyano group of **T9** formed the hydrogen bonds with Asp829 and Asn70, respectively, in addition to the bidentate hydrogen bonds with the hinge region (Fig. 3A and B), which might contribute to the improvement on FLT3 inhibitory activity. Switching the amino group of **T7** to the *para* position in the phenyl ring (**T11**) led to an 8-fold decrease in FLT3 inhibitory activity, indicating that the meta-substitution might be preferred. Subsequently, we introduced the substituted amino groups at the *meta* position of phenyl ring. The addition of the *meta*-methylamino (**T12**, IC_{50}: 75.26 nM) and *meta*-acetamido group (**T13**, IC_{50}: 41.02 nM) caused a 6-fold and a 3-fold decrease in the enzymatic activity, respectively, compared with **T7**. This was probably due to the hindrance of hydrogen bonding formation between the amino group and Asp829 when the hydrogen atom of NH_2 was substituted with methyl group (Fig. 3**C**). Similarly, fusing the NH_2 with a phenyl ring to form the indole ring (**T14**) might also obstruct the hydrogen binding interaction with Asp829, leading to a 6-fold decrease in FLT3 inhibitory activity (IC_{50}: 71.02 nM). The SARs of *meta*-NH_2 in the benzene ring inspired us to try the carbamoyl group that may also form a favorable interaction with Asp829. As a result, this modification yielded **T15** with both potent FLT3 inhibitory (IC_{50}: 6.7 nM) and antiproliferative (IC_{50}: 0.11 μM) activities, which formed the expected hydrogen bonding interaction with Asp829 (Fig. 3**D**). In contrast, the addition of an methyl group on the carbamoyl group attenuated the enzymatic activity (**T16** and **T17**), which probably interrupted the favored hydrogen bonding interaction with Asp829.

Next, we investigated the impact of hydrophilic moieties on the enzymatic and cellular efficacies when keeping the *meta*-carbamoyl substitution. As data shown in Table 2, switching the piperazine moiety with the open-ring tertiary amine moiety (**T18**) caused a 3-fold decrease in the FLT3 inhibitory activity (IC_{50}: 21.2 nM), and the piperidine moiety (**T19**) also weakened the FLT3 inhibitory activity by two folds (IC_{50}: 12.2 nM). However, both the morpholine (**T20**) and *N*-methyl piperazine (**T21**) moieties showed almost equivalent effects on the enzymatic and cellular activities when compared with the piperazine moiety (**T15**), probably due to the existence of favorable interactions between the terminal heteroatoms of hydrophilic moieties and the waters outside the binding pocket.

We further introduced small groups on the phenyl linker to form favorable interactions with the surrounding hydrophobic residue side chains. In general, the addition of the fluorine atom (**T22**), methyl (**T23**) or methoxyl (**T24**) group increased the FLT3 inhibitory activity in various degrees and had different effects on the cellular efficacy (Table 2). Compound **T22** exhibited the increased FLT3 inhibitory activity but similar antiproliferative efficacy against MV4-11 cells, compared with **T15**. Compound **T23**, with the methyl substitution, displayed the most potent cellular activity (IC_{50}: 0.029 μM) in this kind of compounds; while compound **T24** with the methoxyl substitution, showed the most potent inhibitory activity against FLT3 (IC_{50}: 0.41 nM), suggesting that the small substituents were beneficial in improving both the enzymatic and cellular activities.

2.4. Molecular dynamics study

To study the binding mode of compound **T24** with FLT3 precisely, we docked it into the "DFG-in" FLT3 structure and simulated the resulting complex using the molecular dynamics (MD) method. As **Fig. S1**

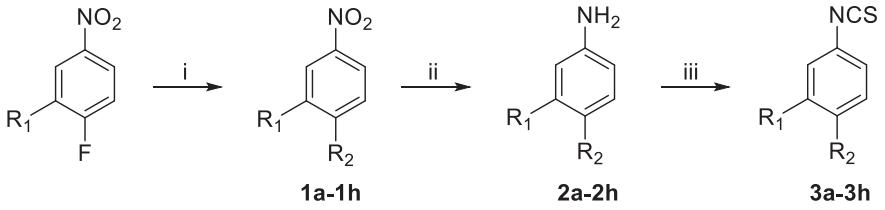

1a-1h **2a-2h** **3a-3h**

1a: R_1 = H, R_2 = 4-(*tert*-butoxycarbonyl)piperazin-1-yl;
1b: R_1 = H, R_2 = diethylamino;
1c: R_1 = H, R_2 = piperidin-1-yl;
1d: R_1 = H, R_2 = morpholino;
1e: R_1 = H, R_2 = 4-methylpiperazin-1-yl;
1f: R_1 = F, R_2 = 4-(*tert*-butoxycarbonyl)piperazin-1-yl;
1g: R_1 = methyl, R_2 = 4-(*tert*-butoxycarbonyl)piperazin-1-yl;
1h: R_1 = methoxyl, R_2 = 4-(*tert*-butoxycarbonyl)piperazin-1-yl;

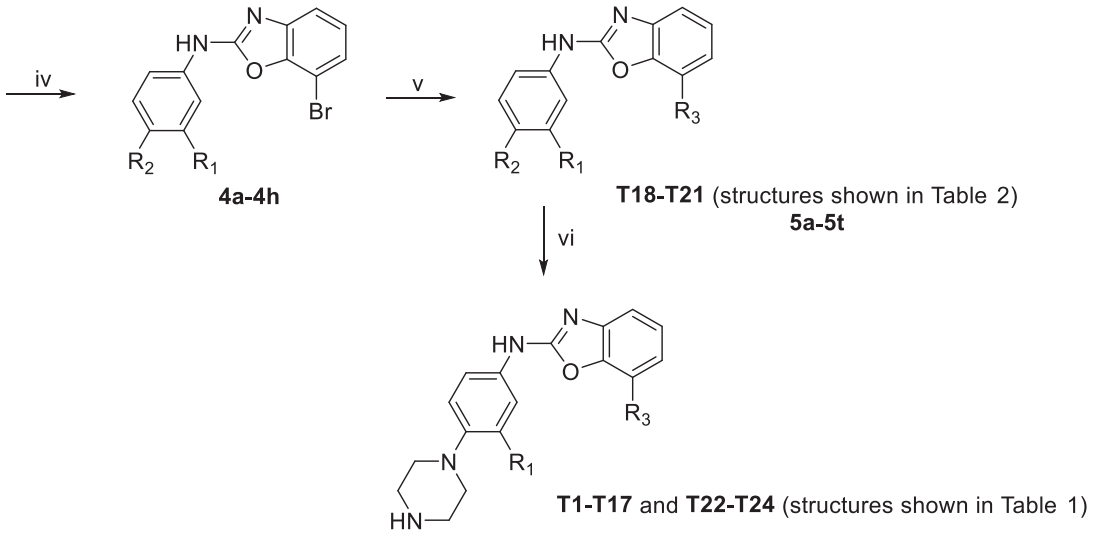

4a-4h

T18-T21 (structures shown in Table 2)
5a-5t

T1-T17 and **T22-T24** (structures shown in Table 1)

5a: R_1 = H, R_2 = 4-(*tert*-butoxycarbonyl)piperazin-1-yl, R_3 = 1,2,3,6-tetrahydropyridine-4-yl;
5b: R_1 = H, R_2 = 4-(*tert*-butoxycarbonyl)piperazin-1-yl, R_3 = 3,6-dihydro-2*H*-pyran-4-yl;
5c: R_1 = H, R_2 = 4-(*tert*-butoxycarbonyl)piperazin-1-yl, R_3 = phenyl;
5d: R_1 = H, R_2 = 4-(*tert*-butoxycarbonyl)piperazin-1-yl, R_3 = pyridin-3-yl;
5e: R_1 = H, R_2 = 4-(*tert*-butoxycarbonyl)piperazin-1-yl, R_3 = pyridin-4-yl;
5f: R_1 = H, R_2 = 4-(*tert*-butoxycarbonyl)piperazin-1-yl, R_3 = 1*H*-pyrazol-4-yl;
5g: R_1 = H, R_2 = 4-(*tert*-butoxycarbonyl)piperazin-1-yl, R_3 = 3-aminophenyl;
5h: R_1 = H, R_2 = 4-(*tert*-butoxycarbonyl)piperazin-1-yl, R_3 = 3-methoxyphenyl;
5i: R_1 = H, R_2 = 4-(*tert*-butoxycarbonyl)piperazin-1-yl, R_3 = 3-cyanophenyl;
5j: R_1 = H, R_2 = 4-(*tert*-butoxycarbonyl)piperazin-1-yl, R_3 = 3-chlorophenyl;
5k: R_1 = H, R_2 = 4-(*tert*-butoxycarbonyl)piperazin-1-yl, R_3 = 4-aminophenyl;
5l: R_1 = H, R_2 = 4-(*tert*-butoxycarbonyl)piperazin-1-yl, R_3 = 3-(methylamino)phenyl;
5m: R_1 = H, R_2 = 4-(*tert*-butoxycarbonyl)piperazin-1-yl, R_3 = 3-acetamidophenyl;
5n: R_1 = H, R_2 = 4-(*tert*-butoxycarbonyl)piperazin-1-yl, R_3 = 1*H*-indol-4-yl;
5o: R_1 = H, R_2 = 4-(*tert*-butoxycarbonyl)piperazin-1-yl, R_3 = 3-carbamoylphenyl;
5p: R_1 = H, R_2 = 4-(*tert*-butoxycarbonyl)piperazin-1-yl, R_3 = 3-(methylcarbamoyl)phenyl;
5q: R_1 = H, R_2 = 4-(*tert*-butoxycarbonyl)piperazin-1-yl, R_3 = 2-(methylcarbamoyl)pyridin-4-yl;
5r: R_1 = F, R_2 = 4-(*tert*-butoxycarbonyl)piperazin-1-yl, R_3 = 3-carbamoylphenyl;
5s: R_1 = methyl, R_2 = 4-(*tert*-butoxycarbonyl)piperazin-1-yl, R_3 = 3-carbamoylphenyl;
5t: R_1 = methoxyl, R_2 = 4-(*tert*-butoxycarbonyl)piperazin-1-yl, R_3 = 3-carbamoylphenyl;

Scheme 1. Synthesis of compound **T1**-**T24**. Reagents and conditions: (i) DMSO, K_2CO_3, 80 °C, *tert*-butyl piperazine-1-carboxylate or diet-hylamine or piperidine or morpholine; (ii) FeO(OH)/C, 80% $NH_2NH_2{\cdot}H_2O$, 95% EtOH; (iii) 1,1′-thiocarbonyldiimidazole, DCM, r.t.; (iv) a) 2-amino-6-bromophenol, DMF, r.t.; b) $CuCl_2$, K_2CO_3, DMF, r.t.; (v) pd(dppf)$_2Cl_2$, Na_2CO_3, dimethyl ether, H_2O, R_3–B(OH)$_2$ or R_3–Boric acid esters; (vi) CF_3COOH, DCM, r.t.

shown, the total energy, potential energy, pressure, temperature and volume of the whole MD system sustained stable during the simulation. FLT3 achieved an equilibrium after 10 ns MD run, and the conformation of compound **T24** balanced fast after only 5 ns MD run (Fig. 4). Thus, we performed the whole-time analysis of the protein–ligand interactions in that 10-ns MD run. It was observed that Cys694, Arg815,

Table 1

Optimization on the benzo[*d*]oxazole moiety.

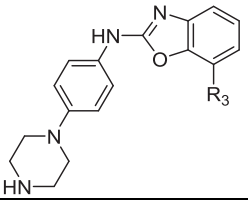

ID	R_3	FLT3-ITD Inhibitory activity [a]	MV4-11 Inhibitory activity
LT-793–323	H	500	25.19%[b]
T1	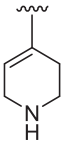	69.51	2.70[c]
T2	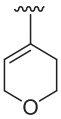	17.60	1.66[c]
T3	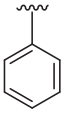	38.52	44.63%[b]
T4	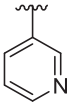	21.22	1.11[c]
T5	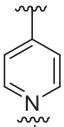	30.41	1.54[c]
T6	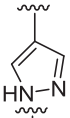	57.04	2.26[c]
T7	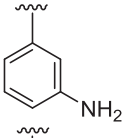	12.02	1.29[c]
T8	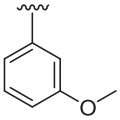	9.16	0.41[c]
T9	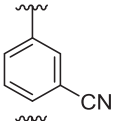	1.02	0.72[c]
T10	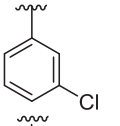	3.81	1.08[c]
T11	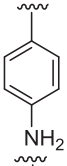	97.30	1.56[c]
T12	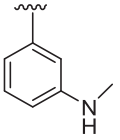	75.26	0.35[c]
T13	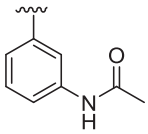	41.02	39.7%[b]
T14	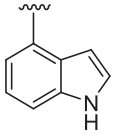	71.02	1.54[c]
T15	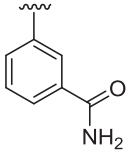	6.7	0.11[c]
T16	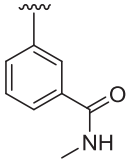	40.98	0.96[c]
T17	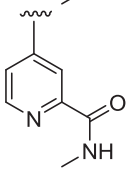	40.10	54.78%[b]
FN-1501	/	0.27	0.015[c]

[a] IC_{50} (nM).
[b] Inhibitory rate at 1 μM.
[c] IC_{50} (μM).

Asn816, Val624, Ala642 and Asp829 contributed more greatly than other residues of FLT3 (Fig. 5A). Among them, two hydrogen bonds between Cys694 and the benzimidazole moiety and the −NH− linker of **T24**, were maintained at 100% and 83% during the analyzed 10-ns MD run, respectively (Fig. 5B), confirming the importance of hydrogen bonding interaction in the hinge region. Another stable hydrogen bond formed between the carbamoyl group of **T24** and Asn816 (78%). In addition, the carbamoyl group were also involved in the direct hydrogen bonding interactions with Arg815 (36%) and Asp829 (20%), as well as the water bridged hydrogen bonding interactions with Arg815 (50%), Asp829 (37%) and Ser618 (25%) (Fig. 5C). The data showed that the carbamoyl group indeed contributed greatly to the interactions with polar residues in the ribose binding area. Only transient ionic interaction was found between **T24** and Tyr693 (Fig. 5A), which suggested the charged piperazine might mainly contribute to the weak and dispersed hydration effect. Besides those polar interactions, many favorable hydrophobic contacts existed between **T24** and the residues Ala620 (68%), Ala642 (63%), Leu818 (38%), Leu616 (33%) and Tyr693 (22%), whose hydrophobic side chains wrapped **T24** within the distance of 3.6 Å (Fig. 5D). The occupations of the intermolecular interactions analyzed above were summarized in **Fig. S2**. Moreover, torsion angles of the rotatable bonds in **T24** were monitored during 10–20 ns MD run. **Fig. S3** showed that the benzimidazole scaffold, carbamoyl group and two benzene linkers kept in a relatively stable state except the methoxy group and piperazine moiety, which was

Table 2
Optimization on the hydrophilic moiety and benzene linker.

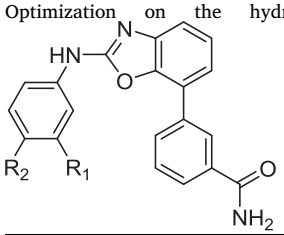

ID	R_1	R_2	FLT3-ITD Inhibitory activity	MV4-11 Inhibitory activity
T18	H	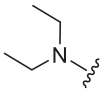	21.2[a]	14.20%[b]
T19	H	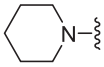	12.2[a]	0.77[c]
T20	H	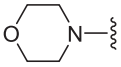	5.29[a]	0.13[c]
T21	H	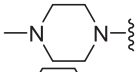	6.02[a]	0.18[c]
T22	F	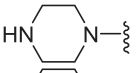	1.09[a]	0.12[c]
T23		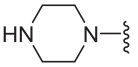	0.97[a]	0.029[c]
T24		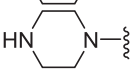	0.41[a]	0.037[c]
FN-1501	/	/	0.27[a]	0.015[c]

[a] IC_{50} (nM).
[b] Inhibitory rate at 1 μM.
[c] IC_{50} (μM).

consistent with the small RMSD fluctuation of backbone atoms of **T24** (Fig. 4), suggesting that the protein-ligand recognition achieved a steady state. We then clustered the conformations of **T24** in 10–20 ns MD run to comprehend its 3D protein-ligand binding mode. As shown in Fig. 6, the cluster analysis generated two representative binding modes, in which the carbamoyl group formed the hydrogen bonding interaction directly with different residues including R815, N816 or D829, or through the bridge of water molecule. Overall, the data from the analyses of MD simulation consolidated our design rationale and agreed well with the SAR conclusion. Binding mode of **T24** from the MD simulation could provide good reference to new FLT3 inhibitor research. Besides, considering that small molecules could bind to both "DFG-in" and "DFG-out" kinases [19], compound **T24** was docked to the FLT3 with "DFG-out" conformation (PDB code: 4XUF). As shown in Figs. S4, 24 bound to the "DFG-out" FLT3 in a similar mode with the its binding mode in the "DFG-in" FLT3. However, an extra π–π interaction was seen between the carbamoyl substituted phenyl ring and Phe830. This was due to the phenyl ring of Phe830 flipped out, and thus facilitated the formation of paralleled phenyl rings.

3. Conclusion

In summary, the structure-based molecular design and SAR studies on benzo[*d*]oxazole-2-amine derivatives led to the discovery of potent FLT3 inhibitors, which showed the strong antiproliferative efficacy against MV4-11 cells. Among these compounds, **T24** was the most promising one, which displayed the potent inhibitory activities in both FLT3-ITD kinase (IC_{50}: 0.41 nM) and MV4-11 cell line levels (IC_{50}: 0.037 μM). Moreover, the binding mode of **T24** with FLT3 was proposed using the MD simulation method, providing the molecule-design rationale for the additional medicinal chemistry. Therefore, compound **T24** represents a new scaffold for further discovery of FLT3-ITD inhibitors in the AML therapy.

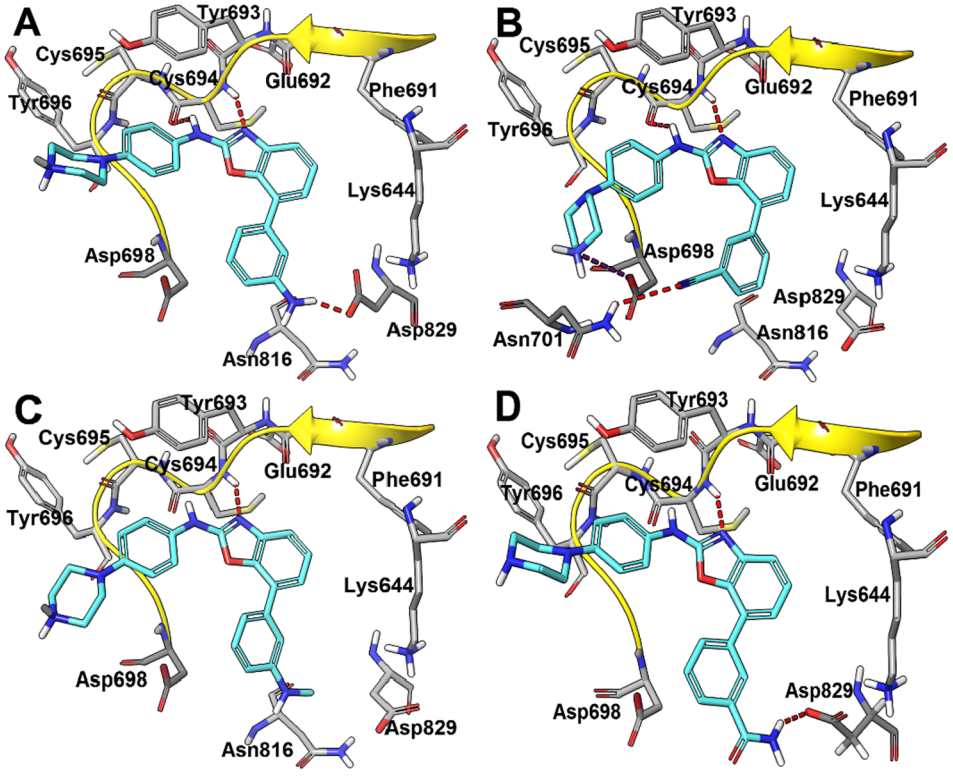

Fig. 3. Bind modes of compound **T7** (A), **T9** (B), **T12** (C) and **T15** (D) with FLT3 homology model from the flexible molecular docking simulations. The color and shape representations are the same as those in Fig. 2.

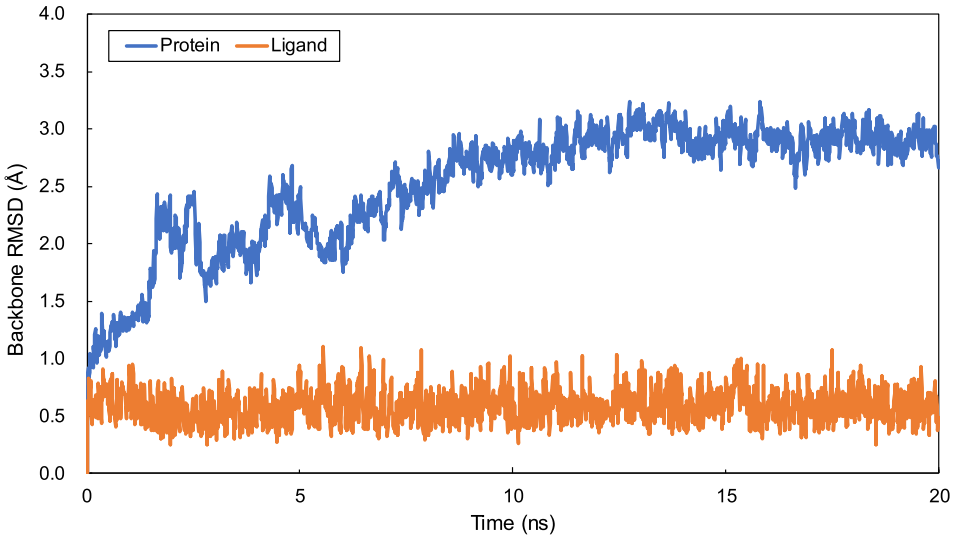

Fig. 4. Average root means square deviation (RMSD) of backbone atoms of the FLT3 protein and compound **T24** during the MD simulation.

4. Experiments

Commercially available materials were used without further purification unless otherwise specified. NMR spectra were recorded on a Bruker AVANCE AV-300 spectrometer (300 MHz for 1H; Bruker, Billerica, MA) or Mass spectra were obtained on an Agilent 1100 LC/MSD mass spectrometer (Agilent, Santa Clara, CA). All reactions were monitored by the TLC (Silica gel GF254, Merck, Kenilworth, NJ), and spots were visualized with the UV light or iodine. The purity of the biologically evaluated compounds were > 95% as determined by HPLC.

4.1. Synthesis

4.1.1. Step 1 Tert-butyl 4-(4-nitrophenyl)piperazine-1-carboxylate (1a)

To a solution of 1-fluoro-4-nitrobenzene (5 g, 35.5 mmol) in DMSO (100 mL) was added K_2CO_3 (14.6 g, 106.4 mmol) at room temperature. And a solution of *tert*-butyl piperazine-1-carboxylate (3.5 g, 35.5 mmol) in DMSO (50 mL) was added dropwise to the mixture at 0 °C. The reaction mixture was stirred at 80 °C for 8 h. Water (500 mL) was added to quench the reaction. The precipitated solid was collected on a filter and dried under reduced pressure to give **1a** (8.0 g, yield 73.5%) without further purification. MS *m/z*: 308.2 $[M+H]^+$. The crude product was delivered directly to the next step.

4.1.2. N,N-diethyl-4-nitroaniline (1b)

Compound **1b** was prepared from diethylamine using the procedure described in step 1 for **1a**. MS *m/z*: 195.5 $[M+H]^+$. The crude product was delivered directly to the next step.

4.1.3. 1-(4-Nitrophenyl)piperidine (1c)

Compound **1c** was prepared from piperidine using the procedure described in step 1 for **1a**. MS *m/z*: 207.2 $[M+H]^+$. The crude product was delivered directly to the next step.

4.1.4. 4-(4-Nitrophenyl)morpholine (1d)

Compound **1d** was prepared from morpholine using the procedure described in step 1 for **1a**. MS *m/z*: 209.5 $[M+H]^+$. The crude product was delivered directly to the next step.

4.1.5. 1-Methyl-4-(4-nitrophenyl)piperazine (1e)

Compound **1e** was prepared from 1-methylpiperazine using the procedure described in step 1 for **1a**. MS *m/z*: 222.5 $[M+H]^+$. The crude product was delivered directly to the next step.

4.1.6. Tert-butyl 4-(2-fluoro-4-nitrophenyl)piperazine-1-carboxylate (1f)

Compound **1f** was prepared from *tert*-butyl piperazine-1-carboxylate and 1,2-difluoro-4-nitroben zene using the procedure described in step 1 for **1a**. MS *m/z*: 326.5 $[M+H]^+$. The crude product was delivered directly to the next step.

4.1.7. Tert-butyl 4-(2-methyl-4-nitrophenyl)piperazine-1-carboxylate (1g)

Compound **1g** was prepared from *tert*-butyl piperazine-1-carboxylate and 1-fluoro-2-methyl-4- nitrobenzene using the procedure described in step 1 for **1a**. MS *m/z*: 322.5 $[M+H]^+$. The crude product was delivered directly to the next step.

4.1.8. Tert-butyl 4-(2-methoxy-4-nitrophenyl)piperazine-1-carboxylate (1h)

Compound **1 h** was prepared from *tert*-butyl piperazine-1-carboxylate and 1-fluoro-2-methoxy-4- nitrobenzene using the procedure described in step 1 for **1a**. MS *m/z*: 338.5 $[M+H]^+$. The crude product was delivered directly to the next step.

4.1.9. Step 2 Tert-butyl 4-(4-aminophenyl)piperazine-1-carboxylate (2a)

To a solution of **1a** (5 g, 22.5 mmol) in 95% ethanol (100 mL) was added goethite (FeO(OH))/C (1.0 g) at room temperature. And a solution of 80% hydrazine hydrate (25 mL, 400 mmol) in 95% ethanol (50 mL) was added dropwise to the mixture at 0 °C. The reaction mixture was stirred at 80 °C for 4 h. The solvent was removed in vacuo to give **2a** (3.8 g, yield 74.5%). MS *m/z*: 278.2 $[M+H]^+$.

4.1.10. N^1,N^1-diethylbenzene-1,4-diamine (2b)

Compound **2b** was prepared from **1b** using the procedure described in step 2 for **2a**. MS *m/z*: 165.5 $[M+H]^+$. The crude product was delivered directly to the next step.

4.1.11. 4-(Piperidin-1-yl)aniline (2c)

Compound **2c** was prepared from **1c** using the procedure described in step 2 for **2a**. MS *m/z*: 177.5 $[M+H]^+$. The crude product was delivered directly to the next step.

4.1.12. 4-Morpholinoaniline (2d)

Compound **2d** was prepared from **1d** using the procedure described in step 2 for **2a**. MS *m/z*: 179.5 $[M+H]^+$. The crude product was delivered directly to the next step.

4.1.13. 4-(4-Methylpiperazin-1-yl)aniline (2e)

Compound **2e** was prepared from **1e** using the procedure described in step 2 for **2a**. MS *m/z*: 192.5 $[M+H]^+$. The crude product was

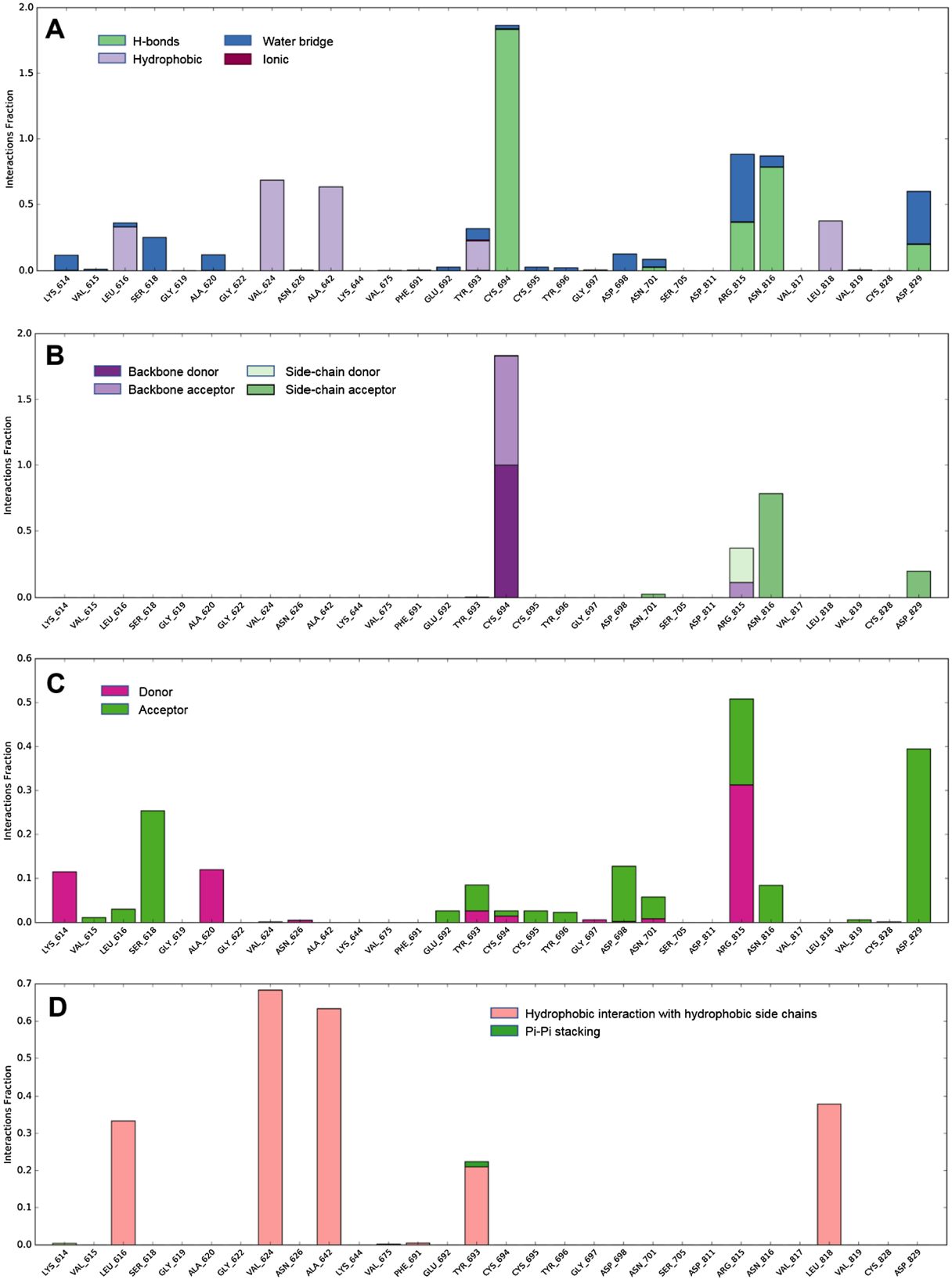

Fig. 5. Stacked bar charts represent the interactions and contacts over the course of the MD trajectory (10–20 ns). A, the overall interactions and contacts; B, the hydrogen bonding interactions; C, water bridged hydrogen bonding interactions; D, the hydrophobic contacts.

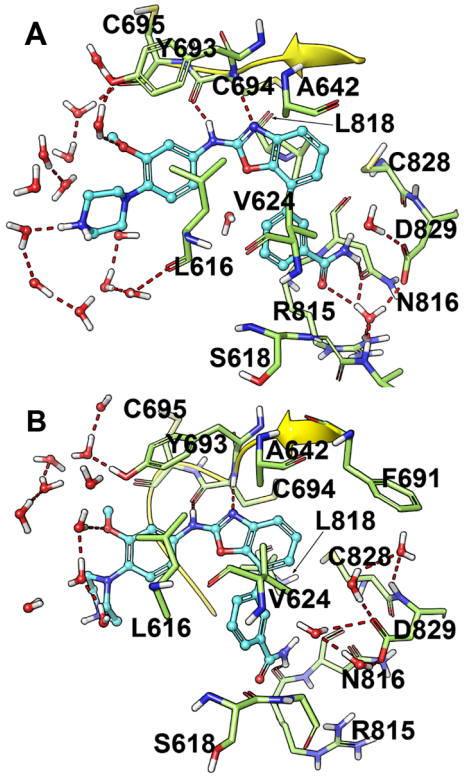

Fig. 6. Two representative binding modes of **T24** with FLT3 from the equilibrium period (10–20 ns) of MD run, in which main differences come from the hydrogen bonding interaction of **T24** with N816 (A) or R815 (B). Red dashed line represents the hydrogen bond. Lemon and cyan sticks represent the residues of FLT3 and **T24**, respectively.

delivered directly to the next step.

*4.1.14. Tert-butyl 4-(4-amino-2-fluorophenyl)piperazine-1-carboxylate (**2f**)*

Compound **2f** was prepared from **1f** using the procedure described in step 2 for **2a**. MS *m/z*: 296.5 $[M+H]^+$. The crude product was delivered directly to the next step.

*4.1.15. Tert-butyl 4-(4-amino-2-methylphenyl)piperazine-1-carboxylate (**2g**)*

Compound **2g** was prepared from **1g** using the procedure described in step 2 for **2a**. MS *m/z*:308.5 $[M+H]^+$. The crude product was delivered directly to the next step.

*4.1.16. Step 3 Tert-butyl 4-(4-isothiocyanatophenyl)piperazine-1-carboxylate (**3a**)*

To a solution of **2a** (1.0 g, 3.6 mmol) in dichloromethane (30 mL) was added 1,1′-thiocarbonyldiimidazole (1.2 g, 7.2 mmol) at room temperature. The reaction mixture was stirred at room temperature for 1 h. The solvent was removed in vacuo and the residue was purified by silica gel chromatography (Developing solvent: petroleum ether (PE)/ethyl acetate (EA) = 20/1) to give **3a** (1.0 g, yield 87.2%). ^{1}H NMR (300 MHz, DMSO-d_6): δ 1.42 (s, 9H), 3.08–3.23 (m, 4H), 3.37–3.52 (m, 4H), 6.96 (d, J = 8.7 Hz, 2H), 7.29 (d, J = 8.7 Hz, 2H).

*4.1.17. N,N-diethyl-4-isothiocyanatoaniline (**3b**)*

Compound **3b** was prepared from **2b** using the procedure described in step 3 for **3a**. ^{1}H NMR (300 MHz, DMSO-d_6) δ 1.07 (t, J = 6.6 Hz, 6H), 3.34 (q, J = 6.5 Hz, 4H), 6.64 (d, J = 7.8 Hz, 2H),7.22 (d, J = 7.7 Hz, 2H).

*4.1.18. 1-(4-Isothiocyanatophenyl)piperidine (**3c**)*

Compound **3c** was prepared from **2c** using the procedure described in step 3 for **3a**. ^{1}H NMR (300 MHz, DMSO-d_6) δ 1.56 (s, 6H), 3.21 (s, 4H), 6.93 (d, J = 8.7 Hz, 2H), 7.25 (d, J = 8.6 Hz, 2H).

*4.1.19. 4-(4-Isothiocyanatophenyl)morpholine (**3d**)*

Compound **3d** was prepared from **2d** using the procedure described in step 3 for **3a**. ^{1}H NMR (300 MHz, DMSO-d_6) δ 3.15 (s, 4H), 3.72 (s, 4H), 6.96 (d, J = 8.7 Hz, 2H),7.30 (d, J = 8.6 Hz, 2H).

*4.1.20. 1-(4-Isothiocyanatophenyl)-4-methylpiperazine (**3e**)*

Compound **3e** was prepared from **2e** using the procedure described in step 3 for **3a**. ^{1}H NMR (300 MHz, $CDCl_3$) δ 2.37 (s, 3H), 2.60–2.54 (m, 4H), 3.60–3.25 (m, 4H), 6.83 (d, J = 9.4 Hz, 1H), 7.26 (s, 1H), 8.13 (d, J = 9.4 Hz, 1H).

*4.1.21. Tert-butyl 4-(2-fluoro-4-isothiocyanatophenyl)piperazine-1-carboxylate (**3f**)*

Compound **3f** was prepared from **2f** using the procedure described in step 3 for **3a**. ^{1}H NMR (300 MHz, DMSO-d_6) δ 1.42 (s, 9H), 2.88–3.09 (m, 4H), 3.38 –3.60 (m, 4H), 7.06 (t, J = 9.1 Hz, 1H), 7.23 (dd, J = 8.7, 1.5 Hz, 1H), 7.39 (dd, J = 13.1, 2.3 Hz, 1H).

*4.1.22. Tert-butyl 4-(4-isothiocyanato-2-methylphenyl)piperazine-1-carboxylate (**3g**)*

Compound **3g** was prepared from **2g** using the procedure described in step 3 for **3a**. The crude product was delivered directly to the next step.

*4.1.23. Tert-butyl 4-(4-isothiocyanato-2-methoxyphenyl)piperazine-1-carboxylate (**3h**)*

Compound **3h** was prepared from **2h** using the procedure described in step 3 for **3a**. ^{1}H NMR (300 MHz, DMSO-d_6) δ 1.41 (s, 9H), 2.97–2.85 (m, 4H), 3.54–3.34 (m, 4H), 3.81 (s, 3H), 6.88 (d, J = 8.5 Hz, 1H), 6.97 (dd, J = 8.4, 2.2 Hz, 1H), 7.06 (d, J = 2.1 Hz, 1H).

*4.1.24. Step 4 Tert-butyl 4-(4-((7-bromobenzo[d]oxazol-2-yl)amino)phenyl) piperazine-1-carboxylate (**4a**)*

To a solution of **3a** (1.0 g, 3.1 mmol) in DMF (30 mL) was added 2-amino-6-bromophenol (0.6 g, 3.4 mmol) at room temperature. The reaction mixture was stirred at room temperature for 14 h. Then, to the reaction mixture was added $CuCl_2$ (0.01 g, 0.074 mmol) and K_2CO_3 (1.2 g, 8.7 mmol). The reaction mixture was stirred at room temperature for another 14 h. Water (100 mL) was added to quench the reaction, and the mixture was extracted with ethyl acetate (30 mL × 3). The combined organic layer was dried over $MgSO_4$. The solvent was removed in vacuo. The residue was purified by silica gel chromatography (Developing solvent: PE/EA = 5/1) to give **4a** (0.55 g, yield 38.6%). ^{1}H NMR (300 MHz, DMSO-d_6): δ 1.42 (s, 9H), 3.03 (s, 4H), 3.47 (s, 4H), 7.00 (d, J = 8.6 Hz, 2H), 7.15 (t, J = 8.7 Hz, 1H), 7.28 (d, J = 7.8 Hz, 1H), 7.40 (d, J = 7.6 Hz, 1H), 7.60 (d, J = 8.6 Hz, 2H), 10.69 (s, 1H). MS *m/z*: 473.2 $[M+H]^+$.

*4.1.25. N^1-(7-bromobenzo[d]oxazol-2-yl)-N^4,N^4-diethylbenzene-1,4-diamine (**4b**)*

Compound **4b** was prepared from **3b** using the procedure described in step 4 for **4a**. ^{1}H NMR (300 MHz, DMSO-d_6): δ 1.07 (t, J = 7.0 Hz, 6H), 3.30 (dd, J = 11.9, 4.8 Hz, 4H), 6.70 (d, J = 9.1 Hz, 2H), 7.13 (t, J = 7.9 Hz, 1H), 7.25 (dd, J = 8.1, 0.9 Hz, 1H), 7.35 (dd, J = 7.7, 0.9 Hz, 1H), 7.50 (d, J = 9.1 Hz, 2H), 10.47 (s, 1H). MS *m/z*: 360.2 $[M+H]^+$.

*4.1.26. 7-Bromo-N-(4-(piperidin-1-yl)phenyl)benzo[d]oxazol-2-amine (**4c**)*

Compound **4c** was prepared from **3c** using the procedure described in step 4 for **4a**. ^{1}H NMR (300 MHz, DMSO-d_6): δ 1.57 (d, J = 31.0 Hz, 6H),3.06 (s, 4H), 6.96 (s, 2H), 7.16 (s, 1H), 7.27 (s, 1H), 7.39 (s, 1H),

7.56 (s, 2H), 10.64 (s, 1H). MS *m/z*: 372.2 $[M+H]^+$.

*4.1.27. 7-Bromo-N-(4-morpholinophenyl)benzo[d]oxazol-2-amine (**4d**)*

Compound **4d** was prepared from **3d** using the procedure described in step 4 for **4a**. ^{1}H NMR (300 MHz, DMSO-d_6): δ 3.08 (s, 4H), 3.77 (s, 4H), 7.00 (s, 2H), 7.18 (s, 1H), 7.30 (s, 1H), 7.42 (s, 1H), 7.63 (s, 2H), 10.71 (s, 1H). MS *m/z*: 374.2 $[M+H]^+$.

*4.1.28. 7-Bromo-N-(4-(4-methylpiperazin-1-yl)phenyl)benzo[d]oxazol-2-amine (**4e**)*

Compound **4e** was prepared from **3e** using the procedure described in step 4 for **4a**. ^{1}H NMR (300 MHz, DMSO-d_6): δ 2.24 (s, 3H), 2.50 (s, 4H), 3.09 (s, 4H), 6.98 (s, 2H), 7.17 (s, 1H), 7.29 (s, 1H), 7.41 (s, 1H), 7.58 (s, 2H), 10.68 (s, 1H). MS *m/z*:387.2 $[M+H]^+$.

*4.1.29. Tert-butyl 4-(4-((7-bromobenzo[d]oxazol-2-yl)amino)-2-fluorophenyl) piperazine-1-carboxylate (**4f**)*

Compound **4f** was prepared from **3f** using the procedure described in step 4 for **4a**. ^{1}H NMR (300 MHz, DMSO-d_6): δ 1.42 (s, 9H), 2.91 (s, 4H), 3.47 (s, 4H), 3.47 (s, 4H), 7.01 – 7.23 (m, 2H), 7.35 (dd, J = 14.9, 8.2 Hz, 2H), 7.46 (d, J = 7.7 Hz, 1H), 7.69 (d, J = 14.4 Hz, 1H), 11.01 (s, 1H). MS *m/z*: 491.2 $[M+H]^+$.

*4.1.30. Tert-butyl 4-(4-((7-bromobenzo[d]oxazol-2-yl)amino)-2-methylphenyl) piperazine-1-carboxylate (**4g**)*

Compound **4g** was prepared from **3g** using the procedure described in step 4 for **4a**. ^{1}H NMR (300 MHz, DMSO-d_6): δ 1.43 (s, 9H), 2.28 (s, 3H), 2.75 (s, 4H), 3.46 (s, 4H), 7.06 (d, J = 9.4 Hz, 1H), 7.16 (t, J = 7.9 Hz, 1H), 7.30 (dd, J = 8.1, 0.9 Hz, 1H), 7.43 (dd, J = 7.7, 0.9 Hz, 1H), 7.53 (d, J = 6.4 Hz, 2H), 10.75 (s, 1H). MS *m/z*: 487.2 $[M+H]^+$.

*4.1.31. Step 5 Tert-butyl 4-(4-((7-(1,2,3,6-tetrahydropyridin-4-yl)benzo [d]oxazol-2-yl)amino)phenyl)piperazine-1-carboxylate (**5a**)*

To a suspension of **4a** (0.1 g, 0.21 mmol) and (1-(*tert*-butoxycarbonyl)-1,2,3,6-tetrahydropyridin-4-yl)boronic acid (0.057 g, 0.25 mmol) in dimethyl ether (DME)/H_2O (4 mL) were added Na_2CO_3 (0.06 g, 0.63 mmol) and $Pd(dppf)_2Cl_2$ (0.034g, 0.04 mmol) under argon atmosphere, which was allowed to react at 100 °C for 8 h. After cooling, water (10 mL) was added to the reaction mixture, and the mixture was extracted with ethyl acetate (15 mL × 3). The organic layer was dried over $MgSO_4$. The solvent was removed in vacuo and the residue was purified by silica gel chromatography (Developing solvent: PE/EA = 3/1) to give **5a** (0.09 g, yield 75.2%). ^{1}H NMR (300 MHz, DMSO-d_6): δ 1.42 (s, 9H), 1.44 (s, 9H), 2.60 (s, 2H), 3.02 (s, 4H), 3.47 (s, 4H), 3.59 (s, 2H), 4.08(s, 2H), 6.52 (s, 1H), 7.00 (d, J = 8.6 Hz, 2H), 7.08 (t, J = 7.5 Hz, 1H), 7.32 (d, J = 7.9 Hz, 1H), 7.62 (d, J = 8.6 Hz, 2H), 10.43 (s, 1H). MS *m/z*: 576.3 $[M+H]^+$.

*4.1.32. Tert-butyl 4-(4-((7-(3,6-dihydro-2H-pyran-4-yl)benzo[d]oxazol-2-yl)amino)phenyl)piperazine-1-carboxylate (**5b**)*

Compound **5b** was prepared from **4a** and 2-(3,6-dihydro-*2H*-pyran-4-yl)-4,4,5,5-tetramethyl-1,3,2-dioxaborolane using the procedure described in step 5 for **5a**. ^{1}H NMR (300 MHz, DMSO-d_6): δ 1.42 (s, 9H), 2.58 (s, 2H), 3.02 (s, 4H), 3.47 (s, 4H), 3.88 (t, J = 5.3 Hz, 2H), 4.38 (s, 2H), 6.60 (s, 1H), 7.00 (d, J = 8.9 Hz, 2H), 7.09 (t, J = 7.8 Hz, 1H), 7.19 (t, J = 7.7 Hz, 1H), 7.32 (d, J = 7.5 Hz, 1H), 7.62 (d, J = 8.7 Hz, 2H), 10.43 (s, 1H). MS *m/z*: 477.5 $[M+H]^+$.

*4.1.33. Tert-butyl 4-(4-((7-phenylbenzo[d]oxazol-2-yl)amino)phenyl)piperazine -1-carboxylate (**5c**)*

Compound **5c** was prepared from **4a** and phenylboronic acid pinacol ester using the procedure described in step 5 for **5a**. ^{1}H NMR (300 MHz, DMSO-d_6): δ 1.42 (s, 9H), 3.03 (s, 4H), 3.47 (s, 4H), 7.00 (d, J = 8.6 Hz, 2H), 7.22–7.37 (m, 2H), 7.37–7.48 (m, 2H), 7.54 (t, J = 7.5 Hz, 2H), 7.65 (d, J = 8.5 Hz, 2H), 7.87 (d, J = 7.8 Hz, 2H), 10.50 (s, 1H). MS *m/z*: 471.1 $[M+H]^+$.

*4.1.34. Tert-butyl 4-(4-((7-(pyridin-3-yl)benzo[d]oxazol-2-yl)amino)phenyl) piperazine-1-carboxylate (**5d**)*

Compound **5d** was prepared from **4a** and 3-(4,4,5,5-Tetramethyl-1,3,2-dioxaborolan-2-yl)pyridine using the procedure described in step 5 for **5a**. ^{1}H NMR (300 MHz, DMSO-d_6): δ 1.42 (s, 9H), 3.03 (s, 4H), 3.03 (s, 4H), 3.47 (s, 4H), 7.01 (d, J = 8.7 Hz, 2H), 7.34 (d, J = 7.7 Hz, 1H), 7.42 (d, J = 7.6 Hz, 1H), 7.47 (d, J = 7.6 Hz, 1H), 7.53 – 7.61 (m, 1H), 7.64 (d, J = 8.6 Hz, 2H), 8.27 (d, J = 8.0 Hz, 1H), 8.63 (d, J = 4.5 Hz, 1H), 9.11 (s, 1H), 10.55 (s, 1H). MS *m/z*: 472.1 $[M+H]^+$.

*4.1.35. Tert-butyl 4-(4-((7-(pyridin-4-yl)benzo[d]oxazol-2-yl)amino)phenyl) piperazine-1-carboxylate (**5e**)*

Compound **5e** was prepared from **4a** and 4-(4,4,5,5-Tetramethyl-1,3,2-dioxaborolan −2-yl)pyridine using the procedure described in step 5 for **5a**. ^{1}H NMR (300 MHz, DMSO-d_6): δ 1.43 (s, 9H), 3.04 (s, 4H), 3.47 (s, 4H), 7.01 (d, J = 8.5 Hz, 2H), 7.36 (d, J = 7.7 Hz, 1H), 7.50 (dd, J = 7.4, 4.0 Hz, 2H), 7.65 (d, J = 8.3 Hz, 2H), 7.91 (d, J = 4.9 Hz, 2H), 8.73 (d, J = 4.8 Hz, 2H), 10.59 (s, 1H). MS *m/z*: 472.1 $[M+H]^+$.

*4.1.36. Tert-butyl 4-(4-((7-(1H-pyrazol-4-yl)benzo[d]oxazol-2-yl)amino) phenyl)piperazine-1-carboxylate (**5f**)*

Compound **5f** was prepared from **4a** and 4-pyrazoleboronic acid pinacol ester using the procedure described in step 5 for **5a**. ^{1}H NMR (300 MHz, DMSO-d_6): δ 1.43 (s, 9H), 3.05 (s, 4H), 3.48 (s, 4H), 7.02 (d, J = 8.0 Hz, 2H), 7.23 (t, J = 10.4 Hz, 2H), 7.40 (d, J = 7.4 Hz, 1H), 7.64 (d, J = 7.8 Hz, 2H), 8.13 (s, 1H), 10.39 (s, 1H), 13.16 (s, 1H). MS *m/z*: 460.2 $[M+H]^+$.

*4.1.37. Tert-butyl 4-(4-((7-(3-aminophenyl)benzo[d]oxazol-2-yl)amino) phenyl)piperazine-1-carboxylate (**5g**)*

Compound **5g** was prepared from **4a** and 3-aminophenylboronic acid pinacol ester using the procedure described in step 5 for **5a**. MS *m/z*: 485.7 $[M+H]^+$. The crude product was delivered directly to the next step.

*4.1.38. Tert-butyl 4-(4-((7-(3-methoxyphenyl)benzo[d]oxazol-2-yl)amino) phenyl)piperazine-1-carboxylate (**5h**)*

Compound **5h** was prepared from **4a** and 3-methoxyphenylboronic acid pinacol ester using the procedure described in step 5 for **5a**. MS *m/z*: 500.2 $[M+H]^+$. The crude product was delivered directly to the next step.

*4.1.39. Tert-butyl 4-(4-((7-(3-cyanophenyl)benzo[d]oxazol-2-yl)amino) phenyl)piperazine-1-carboxylate (**5i**)*

Compound **5i** was prepared from **4a** and 3-(4,4,5,5-tetramethyl-1,3,2-dioxaborolan-2-yl) benzonitrile using the procedure described in step 5 for **5a**. ^{1}H NMR (300 MHz, DMSO-d_6): δ 1.43 (s, 9H), 2.97–3.09 (m, 4H), 3.42 – 3.53 (m, 4H), 7.01 (d, J = 9.0 Hz, 2H), 7.32 (t, J = 7.7 Hz, 1H), 7.44 (dd, J = 12.6, 7.2 Hz, 2H), 7.64 (d, J = 8.9 Hz, 2H), 7.75 (t, J = 7.8 Hz, 1H), 7.91 (d, J = 7.8 Hz, 1H), 8.21 (d, J = 8.0 Hz, 1H), 8.33 (s, 1H), 10.54 (s, 1H). MS *m/z*: 496.5 $[M+H]^+$.

*4.1.40. Tert-butyl 4-(4-((7-(3-chlorophenyl)benzo[d]oxazol-2-yl)amino) phenyl)piperazine-1-carboxylate (**5j**)*

Compound **5j** was prepared from **4a** and 2-(3-chlorophenyl)-4,4,5,5-tetramethyl-1,3,2-dioxaborolane using the procedure described in step 5 for **5a**. MS *m/z*: 505.5 $[M+H]^+$.

*4.1.41. Tert-butyl 4-(4-((7-(4-aminophenyl)benzo[d]oxazol-2-yl)amino) phenyl)piperazine-1-carboxylate (**5k**)*

Compound **5k** was prepared from **4a** and 4-aminophenylboronic acid pinacol ester using the procedure described in step 5 for **5a**. MS *m/z*: 485.7 $[M+H]^+$.

*4.1.42. Tert-butyl 4-(4-((7-(3-(methylamino)phenyl)benzo[d]oxazol-2-yl) amino)phenyl)piperazine-1- carboxylate (**5l**)*

Compound **5l** was prepared from **4a** and *N*-methyl-3-(4,4,5,5-tetramethyl-1,3,2-dioxaborolan -2-yl)aniline using the procedure described in step 5 for **5a**. ^{1}H NMR (300 MHz, DMSO-d_6): δ 1.43 (s, 9H), 2.75 (d, J = 4.9 Hz, 3H), 3.03 (s, 4H), 3.47 (s, 4H), 5.70 (d, J = 4.9 Hz, 1H), 6.60 (dd, J = 8.0, 1.5 Hz, 1H), 6.92 (s, 1H), 6.99 (dd, J = 7.4, 5.2 Hz, 3H), 7.15–7.30 (m, 3H), 7.35 (dd, J = 6.6, 2.3 Hz, 1H), 7.63 (d, J = 9.0 Hz, 2H), 10.35 (s, 1H). MS *m/z*: 498.6 $[M+H]^+$.

*4.1.43. Tert-butyl4-(4-((7-(3-acetamidophenyl)benzo[d]oxazol-2-yl) amino)phenyl)piperazine-1-carboxyl ate (**5m**)*

Compound **5m** was prepared from **4a** and 3-(4,4,5,5-Tetramethyl-1,3,2-dioxaborolan-2-yl)acetanilide using the procedure described in step 5 for **5a**. ^{1}H NMR (300 MHz, DMSO-d_6): δ 1.43 (s, 9H), 2.09 (s, 3H), 2.91–3.12 (m, 4H), 3.40–3.54 (m, 4H), 6.99 (d, J = 9.1 Hz, 2H), 7.17–7.24 (m, 1H), 7.30 (dd, J = 10.3, 5.1 Hz, 1H), 7.36–7.42 (m, 1H), 7.45 (d, J = 7.8 Hz, 1H), 7.50 (d, J = 7.7 Hz, 1H), 7.65 (t, J = 7.5 Hz, 3H), 7.98 (s, 1H), 10.03 (s, 1H), 10.40 (s, 1H). MS *m/z*: 528.6 $[M+H]^+$.

*4.1.44. Tert-butyl 4-(4-((7-(1H-indol-4-yl)benzo[d]oxazol-2-yl)amino)phenyl) piperazine-1-carboxylate (**5n**)*

Compound **5n** was prepared from **4a** and4-(4,4,5,5-tetramethyl-1,3,2-dioxaborolan-2-yl)-*1H*-indole using the procedure described in step 5 for **5a**. ^{1}H NMR (300 MHz, DMSO-d_6): δ 1.43 (s, 9H), 3.02 (s, 4H), 3.47 (s, 4H), 6.43 (s, 1H), 6.97 (d, J = 8.8 Hz, 2H), 7.24 (dd, J = 15.1, 7.4 Hz, 2H), 7.31 (d, J = 4.5 Hz, 2H), 7.42 (t, J = 4.2 Hz, 2H), 7.48 (d, J = 7.7 Hz, 1H), 7.63 (d, J = 8.8 Hz, 2H), 10.36 (s, 1H), 11.28 (s, 1H). MS *m/z*: 510.6 $[M+H]^+$.

*4.1.45. Tert-butyl 4-(4-((7-(3-carbamoylphenyl)benzo[d]oxazol-2-yl)amino) phenyl)piperazine-1-carboxylate (**5o**)*

Compound **5o** was prepared from **4a** and 3-(4,4,5,5-tetramethyl-1,3,2-dioxaborolan-2-yl)benzamide using the procedure described in step 5 for **5a**. ^{1}H NMR (300 MHz, DMSO-d_6): δ 1.48 (s, 9H), 3.03–3.14 (m, 4H), 3.45–3.59 (m, 4H), 7.04 (d, J = 8.0 Hz, 2H), 7.41 (dt, J = 21.6, 6.9 Hz, 4H), 7.52–7.54 (m, 1H), 7.67 (t, J = 9.4 Hz, 3H), 7.96 (d, J = 6.8 Hz, 1H), 8.05 (d, J = 6.7 Hz, 2H), 8.36 (s, 1H), 10.43 (s, 1H). MS *m/z*: 528.6 $[M+H]^+$.

*4.1.46. Tert-butyl 4-(4-((7-(3-(methylcarbamoyl)phenyl)benzo[d]oxazol-2-yl)amino)phenyl)piperazine-1-carboxylate (**5p**)*

Compound **5p** was prepared from **4a** and 3-(4,4,5,5-tetramethyl-1,3,2-dioxaborolan-2-yl)benzamide using the procedure described in step 5 for **5a**. ^{1}H NMR (300 MHz, DMSO-d_6): δ 1.43 (s, 9H), 2.83 (d, J = 4.5 Hz, 3H), 2.98–3.08 (m, 4H), 3.46 (d, J = 4.8 Hz, 4H), 7.00 (d, J = 9.0 Hz, 2H), 7.28–7.40 (m, 2H), 7.43 (d, J = 7.3 Hz, 1H), 7.63 (dd, J = 12.5, 5.3 Hz, 3H), 7.87 (d, J = 7.9 Hz, 1H), 8.00 (d, J = 7.7 Hz, 1H), 8.26 (s, 1H), 8.57 (d, J = 4.5 Hz, 1H), 10.49 (s, 1H). MS *m/z*: 528.6 $[M+H]^+$.

*4.1.47. Tert-butyl 4-(4-((7-(2-(methylcarbamoyl)pyridin-4-yl)benzo[d] oxazol-2-yl)amino)phenyl)piperazine-1-carboxylate (**5q**)*

Compound **5q** was prepared from **4a** and (2-(methylcarbamoyl) pyridin-4-yl)boronic acid using the procedure described in step 5 for **5a**. ^{1}H NMR (300 MHz, DMSO-d_6): δ 1.43 (s, 9H), 2.88 (d, J = 4.8 Hz, 3H), 2.96–3.16 (m, 4H), 3.40–3.54 (m, 4H), 7.01 (d, J = 9.1 Hz, 2H), 7.37 (t, J = 7.8 Hz, 1H), 7.52 (t, J = 7.1 Hz, 2H), 7.65 (d, J = 9.0 Hz, 2H), 8.06 (dd, J = 5.1, 1.8 Hz, 1H), 8.48 (d, J = 1.2 Hz, 1H), 8.77 (d, J = 5.1 Hz, 1H), 8.86 (d, J = 4.8 Hz, 1H), 10.59 (s, 1H). MS *m/z*: 529.5 $[M+H]^+$.

*4.1.48. Tert-butyl 4-(4-((7-(3-carbamoylphenyl)benzo[d]oxazol-2-yl)amino)-2-fluorophenyl)piperazine-1-carboxylate (**5r**)*

Compound **5r** was prepared from **4f** and (2-(methylcarbamoyl) pyridin-4-yl)boronic acid using the procedure described in step 5 for **5a**. ^{1}H NMR (300 MHz, DMSO-d_6): δ 1.42 (s, 9H), 2.91 (s, 4H), 3.47 (s, 4H), 3.47 (s, 4H), 7.01–7.23 (m, 2H), 7.35 (dd, J = 14.9, 8.2 Hz, 2H), 7.46 (d, J = 7.7 Hz, 1H), 7.69 (d, J = 14.4 Hz, 1H), 11.01 (s, 1H). MS *m/z*: 491.2 $[M+H]^+$.

*4.1.49. Tert-butyl 4-(4-((7-(3-carbamoylphenyl)benzo[d]oxazol-2-yl)amino)-2-methylphenyl)piperazine-1-carboxylate (**5s**)*

Compound **5s** was prepared from **4g** and (2-(methylcarbamoyl) pyridin-4-yl)boronic acid using the procedure described in step 5 for **5a**. ^{1}H NMR (300 MHz, DMSO-d_6): δ 1.43 (s, 9H), 2.28 (s, 3H), 2.75 (s, 4H), 3.46 (s, 4H), 7.06 (d, J = 9.4 Hz, 1H), 7.16 (t, J = 7.9 Hz, 1H), 7.30 (dd, J = 8.1, 0.9 Hz, 1H), 7.43 (dd, J = 7.7, 0.9 Hz, 1H), 7.53 (d, J = 6.4 Hz, 2H), 10.75 (s, 1H). MS *m/z*: 487.2 $[M+H]^+$.

*4.1.50. Tert-butyl 4-(4-((7-(3-carbamoylphenyl)benzo[d]oxazol-2-yl) amino)-2-methoxyphenyl)piperazine-1-carboxylate (**5t**)*

Compound **5t** was prepared from **4h** and (2-(methylcarbamoyl) pyridin-4-yl)boronic acid using the procedure described in step 5 for **5a**. ^{1}H NMR (300 MHz, DMSO-d_6): δ 1.42 (s, 9H), 2.86 (s, 4H), 3.45 (s, 4H), 3.81 (s, 3H), 6.92 (d, J = 8.6 Hz, 1H), 7.16 (t, J = 7.9 Hz, 1H), 7.23–7.33 (m, 2H), 7.38 (d, J = 2.3 Hz, 1H), 7.41 (dd, J = 7.7, 0.9 Hz, 1H), 10.78 (s, 1H). MS *m/z*: 503.2 $[M+H]^+$.

*4.1.51. Step 6 N-(4-(piperazin-1-yl)phenyl)-7-(1,2,3,6-tetrahydropyridin-4-yl)benzo[d]oxazol-2-amine (**T1**)*

To a solution of **5a** (60 mg, 0.13 mmol) in dichloromethane (3 mL) was added CF_3COOH (0.3 mL) at room temperature. The reaction mixture was stirred at room temperature for 6 h. Saturated aqueous sodium bicarbonate was added to the reaction mixture until the *p*H of solution was 7–8. The precipitated solid was collected on a filter and was further purified by silica gel chromatography (Developing solvent: dichloromethane/MeOH = 10/1) to give **T1** (30 mg, yield 81.8%). ^{1}H NMR (300 MHz, DMSO-d_6): δ 2.75–2.89 (m, 4H), 2.91–3.02 (m, 4H), 3.44 (s, 2H), 6.54 (s, 1H), 6.94 (d, J = 9.0 Hz, 2H), 7.02–7.09 (m, 1H), 7.16 (t, J = 7.7 Hz, 1H), 7.28 (d, J = 7.4 Hz, 1H), 7.60 (d, J = 9.0 Hz, 2H), 10.33 (s, 1H). HRMS-ESI *m/z* $[M+H]^+$, calcd for $C_{22}H_{26}N_5O$: 376.2137, found: 376.2133.

*4.1.52. 7-(3,6-Dihydro-2H-pyran-4-yl)-N-(4-(piperazin-1-yl)phenyl)benzo [d]oxazol-2-amine (**T2**)*

Compound **T2** was prepared from **5b** using the procedure described in step 6 for **T1**. ^{1}H NMR (300 MHz, DMSO-d_6): δ 2.58 (s, 2H), 2.75–2.88 (m, 4H), 2.88–3.03 (m, 4H), 3.88 (t, J = 5.4 Hz, 2H), 4.31 (d, J = 2.5 Hz, 2H), 6.60 (s, 1H), 6.94 (d, J = 8.9 Hz, 2H), 7.09 (d, J = 7.0 Hz, 1H), 7.18 (t, J = 7.7 Hz, 1H), 7.31 (d, J = 7.0 Hz, 1H), 7.59 (d, J = 9.0 Hz, 2H), 10.39 (s, 1H,). HRMS-ESI *m/z* $[M+H]^+$, calcd for $C_{22}H_{25}N_4O_2$: 377.1978, found: 377.1976.

*4.1.53. 7-Phenyl-N-(4-(piperazin-1-yl)phenyl)benzo[d]oxazol-2-amine (**T3**)*

Compound **T3** was prepared from **5c** using the procedure described in step 6 for **T1**. ^{1}H NMR (300 MHz, DMSO-d_6): δ 2.86–2.99 (s, 4H), 3.00–3.11 (s, 4H), 6.97 (d, J = 9.0 Hz, 1H), 7.24–7.36 (m, 1H), 7.37–7.48 (m, 2H), 7.54 (t, J = 7.6 Hz, 1H), 7.64 (d, J = 8.9 Hz, 1H), 7.87 (d, J = 7.4 Hz, 1H),10.47 (s, 1H). HRMS-ESI *m/z* $[M+H]^+$, calcd for $C_{23}H_{23}N_4O$: 371.1872, found: 371.1871.

*4.1.54. N-(4-(piperazin-1-yl)phenyl)-7-(pyridin-3-yl)benzo[d]oxazol-2-amine (**T4**)*

Compound **T4** was prepared from **5d** using the procedure described in step 6 for **T1**. ^{1}H NMR (300 MHz, DMSO-d_6): δ 2.93–2.99 (m, 4H), 3.04–3.10 (m, 4H), 6.98 (d, J = 9.1 Hz, 2H), 7.33 (t, J = 7.7 Hz, 1H), 7.43 (ddd, J = 13.6, 7.7, 1.3 Hz, 2H), 7.54–7.60 (m, 1H), 7.63 (d, J = 9.0 Hz, 2H), 8.37–8.17 (m, 1H), 8.63 (dd, J = 4.8, 1.6 Hz, 1H), 9.09–9.12 (m, 1H), 10.50 (s, 1H). HRMS-ESI *m/z* $[M+H]^+$, calcd for $C_{22}H_{22}N_5O$: 372.1824, found: 372.1820.

*4.1.55. N-(4-(piperazin-1-yl)phenyl)-7-(pyridin-4-yl)benzo[d]oxazol-2-amine (**T5**)*

Compound **T5** was prepared from **5e** using the procedure described in step 6 for **T1**. ^{1}H NMR (300 MHz, DMSO-d_6): δ 2.97–3.05 (m, 4H), 3.08–3.16(m, 4H), 7.00 (d, J = 9.1 Hz, 2H), 7.29–7.31 (m, 1H), 7.49 (d, J = 1.6 Hz, 1H), 7.50–7.55 (m, 1H), 7.64 (d, J = 9.0 Hz, 2H), 7.91 (dd, J = 4.6, 1.6 Hz, 2H), 8.81–8.66 (m, 2H), 10.56 (s, 1H). HRMS-ESI m/z $[M+H]^+$, calcd for $C_{22}H_{22}N_5O$: 372.1824, found: 372.1818.

*4.1.56. N-(4-(piperazin-1-yl)phenyl)-7-(1H-pyrazol-4-yl)benzo[d]oxazol-2-amine (**T6**)*

Compound **T6** was prepared from **5f** using the procedure described in step 6 for **T1**. ^{1}H NMR (300 MHz, DMSO-d_6): δ 3.03–3.15 (m, 4H), 3.03–3.15 (m, 4H),7.06 (d, J = 9.0 Hz, 2H), 7.14–7.29 (m, 2H), 7.41 (d, J = 7.0 Hz, 1H), 7.68 (d, J = 8.9 Hz, 2H), 8.01–8.39 (m, 1H) 10.47 (s, 1H), 13.20 (s, 1H). HRMS-ESI m/z $[M+H]^+$, calcd for $C_{20}H_{21}N_6O$: 361.1777 $[M+H]^+$, found: 361.1780.

*4.1.57. 7-(3-Aminophenyl)-N-(4-(piperazin-1-yl)phenyl)benzo[d]oxazol-2-amine (**T7**)*

Compound **T7** was prepared from **5g** using the procedure described in step 6 for **T1**. ^{1}H NMR (300 MHz, DMSO-d_6): δ 2.87–2.98 (m, 4H), 3.01–3.12 (m, 4H), 5.19 (s, 2H),. 6.62 (d, J = 8.1 Hz, 1H), 6.96 (d, J = 8.1 Hz, 4H), 7.10–7.20 (m, 2H), 7.25 (t, J = 7.6 Hz, 1H), 7.35 (d, J = 7.5 Hz, 1H), 7.63 (d, J = 8.7 Hz, 2H), 10.43 (s, 1H). HRMS-ESI m/z $[M+H]^+$, calcd for $C_{23}H_{24}N_5O$: 386.1981, found: 386.1979.

*4.1.58. 7-(3-Methoxyphenyl)-N-(4-(piperazin-1-yl)phenyl)benzo[d]oxazol-2-amine (**T8**)*

Compound **T8** was prepared from **5h** using the procedure described in step 6 for **T1**. ^{1}H NMR (300 MHz, DMSO-d_6): δ 3.07–3.16 (s, 4H), 3.16–3.23 (s, 4H), 3.85 (s, 3H), 7.01 (d, J = 8.7 Hz, 3H), 7.24–7.38 (m, 2H), 7.38–7.48 (m, 4H), 7.65 (d, J = 8.7 Hz, 2H), 10.48 (s, 1H). HRMS-ESI m/z $[M+H]^+$, calcd for $C_{24}H_{24}N_5O_3$: 401.1978, found: 401.1969.

*4.1.59. 3-(2-((4-(Piperazin-1-yl)phenyl)amino)benzo[d]oxazol-7-yl)benzonitrile (**T9**)*

Compound **T9** was prepared from **5i** using the procedure described in step 6 for **T1**. ^{1}H NMR (300 MHz, DMSO-d_6): δ 2.90 (s, 4H), 3.03 (s, 4H), 6.98 (d, J = 5.2 Hz, 2H), 7.25–7.38 (m, 1H), 7.38–7.51 (m, 2H), 7.63 (d, J = 5.2 Hz, 2H), 7.82–7.69 (m, 1H), 7.90 (s, 1H), 8.18–8.28 (m, 1H), 8.34 (s, 1H), 10.50 (s, 1H). HRMS-ESI m/z $[M+H]^+$, calcd for $C_{24}H_{22}N_5O$: 396.1824, found: 396.1830.

*4.1.60. 7-(3-Chlorophenyl)-N-(4-(piperazin-1-yl)phenyl)benzo[d]oxazol-2-amine (**T10**)*

Compound **T10** was prepared from **5j** using the procedure described in step 6 for **T1**. ^{1}H NMR (300 MHz, MeOD) δ 3.25 (s, 4H), 3.26 (s, 4H), 7.05 (d, J = 9.0 Hz, 2H),7.28–7.34 (m,2H), 7.36 (t, J = 2.9 Hz, 1H), 7.44–7.38 (m, 1H), 7.48 (t, J = 7.9 Hz, 1H), 7.58 (d, J = 8.9 Hz, 2H), 7.77 (d, J = 7.7 Hz, 1H), 7.87–7.92 (m,1H). HRMS-ESI m/z $[M+H]^+$, calcd for $C_{23}H_{22}ClN_4O$: 405.1482, found: 405.1468.

*4.1.61. 7-(4-Aminophenyl)-N-(4-(piperazin-1-yl)phenyl)benzo[d]oxazol-2-amine (**T11**)*

Compound **T11** was prepared from **5k** using the procedure described in step 6 for **T1**. ^{1}H NMR (300 MHz, DMSO-d_6): δ 3.22 (s, 4H), 3.24 (s, 4H), 5.36 (s, 2H), 6.70 (d, J = 8.3 Hz, 2H), 7.03 (d, J = 8.7 Hz, 2H), 7.31–7.18 (m, 3H), 7.60 (d, J = 8.3 Hz, 2H), 7.68 (d, J = 8.7 Hz, 2H), 10.45 (s, 1H). HRMS-ESI m/z $[M+H]^+$, calcd for $C_{23}H_{24}N_5O$: 386.1981, found: 386.1976.

*4.1.62. 7-(3-(Methylamino)phenyl)-N-(4-(piperazin-1-yl)phenyl)benzo[d]oxazol-2-amine (**T12**)*

Compound **T12** was prepared from **5l** using the procedure described in step 6 for **T1**. ^{1}H NMR (300 MHz, DMSO-d_6): δ 2.75 (d, J = 4.9 Hz, 3H), 2.93–3.02 (m, 4H), 3.02–3.15 (m, 4H), 5.68–5.85 (m, 1H), 6.60 (d, J = 8.2 Hz, 1H), 6.92 (s, 1H), 6.99 (t, J = 8.1 Hz, 3H), 7.31–7.16 (m, 3H), 7.33–7.40 (m, 1H), 7.63 (d, J = 8.9 Hz, 2H), 10.41 (s, 1H). HRMS-ESI m/z $[M+H]^+$, calcd for $C_{24}H_{26}N_5O$: 400.2137, found: 400.2136.

*4.1.63. N-(3-(2-((4-(piperazin-1-yl)phenyl)amino)benzo[d]oxazol-7-yl)phenyl)acetamide (**T13**)*

Compound **T13** was prepared from **5m** using the procedure described in step 6 for **T1**. ^{1}H NMR (300 MHz, DMSO-d_6): δ 2.09 (s, 3H), 3.02–3.12 (m, 4H), 3.12–3.20 (m, 4H), 7.00 (d, J = 9.1 Hz, 2H), 7.18–7.25 (m, 1H), 7.30 (t, J = 7.7 Hz, 1H), 7.37–7.54 (m, 3H), 7.65 (d, J = 9.0 Hz, 3H), 8.00 (s, 1H), 10.11 (s, 1H), 10.47 (s, 1H). HRMS-ESI m/z $[M+H]^+$, calcd for $C_{25}H_{26}N_5O_2$: 428.2087, found: 428.2085.

*4.1.64. 7-(1H-indol-4-yl)-N-(4-(piperazin-1-yl)phenyl)benzo[d]oxazol-2-amine (**T14**)*

Compound **T14** was prepared from **5n** using the procedure described in step 6 for **T1**. ^{1}H NMR (300 MHz, DMSO-d_6): δ 3.07–3.16 (m, 4H), 3.16–3.24 (m, 4H), 6.42 (s, 1H), 7.00 (d, J = 9.1 Hz, 2H), 7.16–7.28 (m, 2H), 7.28–7.35 (m, 2H), 7.38–7.51 (m, 1H), 7.65 (d, J = 9.0 Hz, 2H), 10.41 (s, 1H), 11.31 (s, 1H). HRMS-ESI m/z $[M+H]^+$, calcd for $C_{25}H_{24}N_5O$: 410.1981, found: 410.1981.

*4.1.65. 3-(2-((4-(Piperazin-1-yl)phenyl)amino)benzo[d]oxazol-7-yl)benzamide (**T15**)*

Compound **T15** was prepared from **5o** using the procedure described in step 6 for **T1**. ^{1}H NMR (300 MHz, DMSO-d_6): δ 2.75–2.91 (m, 4H), 2.92–3.09 (m, 4H), 6.95 (d, J = 9.0 Hz, 2H), 7.25–7.39 (m, 2H), 7.40 (t, J = 7.5 Hz, 1H), 7,51(s, 1H), 7.56–7.66 (m, 3H), 7.91 (d, J = 7.8 Hz, 1H), 8.00 (d, J = 7.8 Hz, 1H), 8.12 (s, 1H), 8.31 (s, 1H), 10.49 (s, 1H). HRMS-ESI m/z $[M+H]^+$, calcd for $C_{24}H_{24}N_5O_2$: 414.1930, found: 414.1919.

*4.1.66. N-methyl-3-(2-((4-(piperazin-1-yl)phenyl)amino)benzo[d]oxazol-7-yl)benzamide (**T16**)*

Compound **T16** was prepared from **5p** using the procedure described in step 6 for **T1**. ^{1}H NMR (300 MHz, DMSO-d_6): δ 2.83 (d, J = 4.5 Hz, 3H), 2.95–3.05 (s, 4H), 3.06–3.17 (m, 4H), 6.99 (d, J = 9.0 Hz, 2H), 7.24–7.40 (m, 2H), 7.41–7.46 (m, 1H),7.57–7.69 (m, 3H), 7.88 (d, J = 7.9 Hz, 1H), 8.00 (d, J = 7.8 Hz, 1H), 8.27 (s, 1H), 8.52–8.65 (m, 1H), 10.49 (s, 1H). HRMS-ESI m/z $[M+H]^+$, calcd for $C_{24}H_{24}N_5O_2$: 428.2087, found: 428.2077.

*4.1.67. N-methyl-4-(2-((4-(piperazin-1-yl)phenyl)amino)benzo[d]oxazol-7-yl)picolinamide (**T17**)*

Compound **T17** was prepared from **5q** using the procedure described in step 6 for **T1**. ^{1}H NMR (300 MHz, DMSO-d_6): δ 2.88 (d, J = 4.8 Hz, 3H), 2.90–2.95 (m, 4H), 3.01–3.10 (m, 4H), 6.98 (d, J = 9.0 Hz, 2H), 7.36 (t, J = 7.8 Hz, 1H), 7.46–7.56 (m, 2H), 7.64 (d, J = 9.0 Hz, 2H), 8.06 (dd, J = 5.1, 1.8 Hz, 1H), 8.47–8.50 (m, 1H), 8.77 (d, J = 5.2 Hz, 1H), 8.81–8.92 (m,1H), 10.56 (s, 1H). HRMS-ESI m/z $[M+H]^+$, calcd for $C_{24}H_{25}N_6O_2$: 429.2039, found: 429.2040.

*4.1.68. 3-(2-((4-(Diethylamino)phenyl)amino)benzo[d]oxazol-7-yl)benzamide (**T18**)*

Compound **T18** was prepared from **4b** using the procedure described above for **5a**. ^{1}H NMR (300 MHz, DMSO-d_6): δ 1.07 (t, J = 6.9 Hz, 6H), 3.24–3.32(m, 4H), 6.71 (d, J = 9.0 Hz, 2H), 7.25–7.43 (m, 3H), 7.47–7.57 (m, 3H), 7.61 (t, J = 7.8 Hz, 1H), 7.91 (d, J = 7.7 Hz, 1H), 8.00 (d, J = 7.1 Hz, 1H), 8.11 (s, 1H), 8.30 (s, 1H), 10.29 (s, 1H). HRMS-ESI m/z $[M+H]^+$, calcd for $C_{24}H_{25}N_4O_2$: 401.1978, found: 401.1977.

*4.1.69. 3-(2-((4-(Piperidin-1-yl)phenyl)amino)benzo[d]oxazol-7-yl)benzamide (**T19**)*

Compound **T19** was prepared from **4c** using the procedure

described above for **5a**. ^{1}H NMR (300 MHz, DMSO-d_6): δ 1.45–1.56 (m, 2H),1.56–1.71 (m, 4H), 3.00–3.12 (m, 4H), 6.96 (d, J = 9.0 Hz, 2H), 7.28–7.40 (m, 2H), 7.43 (d, J = 7.2 Hz, 1H), 7.51 (s, 1H), 7.56–7.67 (m, 3H), 7.91 (d, J = 7.8 Hz, 1H), 8.00 (d, J = 7.7 Hz, 1H), 8.12 (s, 1H), 8.31 (s, 1H), 10.46 (s, 1H). HRMS-ESI m/z $[M+H]^+$, calcd for $C_{25}H_{25}N_4O_2$: 413.1978, found: 413.1966.

*4.1.70. 3-(2-((4-Morpholinophenyl)amino)benzo[d]oxazol-7-yl) benzamide (**T20**)*

Compound **T20** was prepared from **4d** using the procedure described above for **5a**. ^{1}H NMR (400 MHz, DMSO-d_6): δ 3.01–3.14 (m, 4H), 3.71–3.81 (d, 4H), 6.98 (d, J = 8.7 Hz, 2H), 7.27–7.35 (m, 1H), 7.38 (d, J = 6.6 Hz, 1H), 7.43 (d, J = 6.8 Hz, 1H), 7.50 (s, 1H), 7.59–7.72 (m, 3H), 7.91 (d, J = 6.9 Hz, 1H), 8.00 (d, J = 7.1 Hz, 1H), 8.12 (s, 1H), 8.31 (s, 1H), 10.49 (s, 1H). HRMS-ESI m/z $[M+H]^+$, calcd for $C_{24}H_{23}N_4O_3$: 415.1770, found: 415.1771.

*4.1.71. 3-(2-((4-(4-Methylpiperazin-1-yl)phenyl)amino)benzo[d]oxazol-7-yl)benzamide (**T21**)*

Compound **T21** was prepared from **4e** using the procedure described above for **5a**. ^{1}H NMR (400 MHz, DMSO-d_6): δ 2.27 (s, 3H), 2.51–2.57 (m, 4H), 3.03–3.16 (m, 4H), 6.97 (d, J = 9.1 Hz, 2H), 7.32 (t, J = 7.7 Hz, 1H), 7.38 (dd, J = 7.8, 1.2 Hz, 1H), 7.43 (dd, J = 7.5, 1.2 Hz, 1H), 7.51 (s, 1H), 7.57–7.69 (m, 3H), 7.92 (d, J = 7.8 Hz, 1H), 8.00 (d, J = 7.9 Hz, 1H), 8.12 (s, 1H), 8.31 (s, 1H), 10.48 (s, 1H). HRMS-ESI m/z $[M+H]^+$, calcd for $C_{25}H_{26}N_5O_2$: 428.2087, found: 428.2088.

*4.1.72. 3-(2-((3-Fluoro-4-(piperazin-1-yl)phenyl)amino)benzo[d]oxazol-7-yl)benzamide (**T22**)*

Compound **T22** was prepared from **5r** using the procedure described above for **T1**. ^{1}H NMR (400 MHz, DMSO-d_6): δ 2.93–3.15 (m, 8H), 7.03–7.18 (m, 1H), 7.31–7.39 (m, 1H), 7.39–7.47 (m, 2H), 7.47–7.57 (m, 2H), 7.70 – 7.58 (m, 1H), 7.76 (d, J = 11.4 Hz, 1H), 7.97–7.98 (m, 1H), 7.98–8.07 (m, 1H), 8.14 (s, 1H), 8.32 (s, 1H), 10.83 (s, 1H). HRMS-ESI m/z $[M+H]^+$, calcd for $C_{24}H_{23}FN_5O_2$: 432.1836, found: 432.1831.

*4.1.73. 3-(2-((3-Methyl-4-(piperazin-1-yl)phenyl)amino)benzo[d]oxazol-7-yl)benzamide (**T23**)*

Compound **T23** was prepared from **5s** using the procedure described above for **T1**. ^{1}H NMR (400 MHz, DMSO-d_6): δ 2.67–2.85 (m, 4H), 2.85–3.00 (m, 4H), 7.04 (d, J = 9.1 Hz, 1H), 7.33 (t, J = 7.7 Hz, 1H), 7.39 (d, J = 7.7 Hz, 1H), 7.45 (d, J = 7.5 Hz, 1H), 7.50 (s, 1H), 7.56 (s, 2H), 7.62 (t, J = 7.7 Hz, 1H), 7.92 (d, J = 7.3 Hz, 1H), 8.01 (d, J = 7.3 Hz, 1H), 8.12 (s, 1H), 8.31 (s, 1H), 10.54 (s, 1H). HRMS-ESI m/z $[M+H]^+$, calcd for $C_{25}H_{26}N_5O_2$: 428.2087, found: 428.2079.

*4.1.74. 3-(2-((3-Methoxy-4-(piperazin-1-yl)phenyl)amino)benzo[d] oxazol-7-yl)benzamide (**T24**)*

Compound **T24** was prepared from **5t** using the procedure described above for **T1**. ^{1}H NMR (300 MHz, DMSO-d_6): δ 2.72–3.04 (m, 8H), 3.80 (s, 3H), 6.91 (d, J = 8.4 Hz, 1H), 7.26–7.48 (m, 5H), 7.51 (s, 1H), 7.62 (t, J = 7.7 Hz, 1H), 7.92 (d, J = 7.6 Hz, 1H), 8.01 (d, J = 7.3 Hz, 1H), 8.12 (s, 1H), 8.31 (s, 1H), 10.57 (s, 1H). HRMS-ESI m/z $[M+H]^+$, calcd for $C_{25}H_{26}N_5O_3$: 444.2036, found: 444.2036.

4.2. Biological assay

4.2.1. Kinase assay

Inhibitory rate or IC_{50} values against kinases were determined as previously reported [20]. Generally, the tests were performed at Reaction Biology Corporation using the "HotSpot" assay platform. The kinase and corresponding substrate were mixed with the reaction buffer (20 mM Hepes pH 7.5, 10 mM $MgCl_2$, 1 mM EGTA, 0.02% Brij35, 0.02 mg/mL BSA, 0.1 mM Na_3VO_4, 2 mM DTT, 1% DMSO) at room temperature. Then DMSO solution of compound (starting at 10 μM with 3-fold serial dilution) were added into the kinase reaction mixture at room temperature. After 20 min, the reaction was initiated by addition of a mixture of ATP (Sigma) and ^{33}P ATP (PerkinElmer) to a final concentration of 10 μM, followed by the incubation of 120 min at 25 °C. The kinase activities were detected by filter-binding method. Kinase activity data of test sample were expressed as the percent remaining kinase activity compared to vehicle (DMSO) reactions. The values of IC_{50} were obtained by using Prism (GraphPad Software, San Diego, CA).

4.2.2. Cell Growth Inhibition Assay

The human cancer cell lines were purchased from the American Type Culture Collection (ATCC, Manassas, VA, USA). The MV4-11 cells were maintained in culture media at 37 °C with 5% CO_2 (100 ng/mL IL-3 was added to parental BaF3 cells). Cells were plated in 384-well culture plates (10,000/well). Cell proliferation was determined after treatment with compounds for 72 h. Cell viability was measured by Cell Titer-Glo assay (Promega, USA) following manufacturer's instructions, and luminescence was measured in a multilabel reader (Envision2014, PerkinElmer, USA). The values of IC_{50} were obtained by using Prism.

4.3. Molecular simulation study

4.3.1. Homology modeling

The structure of "DFG-in" FLT3 was constructed using the homology modeling method as described in our previously published paper [22], which was directly used in this work.

4.3.2. Molecular docking

The FLT3 model was prepared with the Protein Preparation Wizard workflow in Schrödinger 2005 platform (Schrödinger, LLC, New York, NY). And ligands were docked into the ATP site using induced-fit docking module based on Glide with default parameters, which allowed the residues within 5 Å of ligand to be flexible. The docked pose with top-ranked Glide score was selected for further simulation.

4.3.3. Molecular dynamics

A MD simulation was performed for the complex of **T24** with FLT3 in Desmond module of Schrödinger, according to the published method [23]. A truncated octahedral box of TIP3P water model was constructed with Na^+ or Cl^- as counter ions. Protein and ligand were charged with OPLS_2005 force field. Prior to MD, energy minimization was conducted with a convergence threshold of 0.01 Kcal/mol/Å. Heating simulation was performed from 0 to 300 K using the Berendsen thermostat with a time step of 1 fs, and a total of 1200 ps heating simulation was accomplished in the NVT ensemble. Equilibrium MD simulation was implemented for 20 ns with a time step of 2 fs, in which NPT ensemble was employed with a temperature fixed at 300 K and pressure at 1.01 bar. We chose a 10 ps recording interval, resulting in a MD trajectory with 2000 unique conformations of **T24**. Default settings were used for all other parameters. The analysis module in Desmond was used to the generated trajectory.

Author contributions

The authors declare no competing financial interest. The manuscript was written through contributions of all authors.

Acknowledgment

We are grateful to the Natural Science Foundation of Jiangsu Province (SBK2016020485), the National Natural Science Foundation of China (81502925), the "Double First-Class University project" (CPU2018GF02) of China Pharmaceutical University, and the Priority Academic Program Development of Jiangsu Higher Education Institutions for financial support. Jiawei Zhang and Wenqianzi Yang

appreciate the College Students Innovation Project for the R&D of Novel Drugs (J1310032) from the National Found for Fostering Talents of Basic Science (NFFTBS).

Appendix A. Supplementary material

Supplementary data to this article can be found online at https://doi.org/10.1016/j.bioorg.2019.103248.

References

[1] C.C. Kumar, Genetic Abnormalities and challenges in the treatment of acute myeloid leukemia, Genes. Cancer 2 (2011) 95–107.
[2] M.R. O'donnell, M.S. Tallman, C.N. Abboud, et al., Acute myeloidleukemia, version 3.2017, NCCN clinical practice guidelines in oncology, J. Natl. Compr. Canc. Netw. 15 (2017) 926–957.
[3] D.L. Stirewalt, J.P. Radich, The role of FLT3 in haematopoietic malignancies, Nat. Rev. Cancer 3 (2003) 650–665.
[4] F. Kuchenbauer, W. Kern, C. Schoch, et al., Detailed analysis of FLT3 expression levels in acute myeloid leukemia, Haematologica. 90 (2005) 1617–1625.
[5] S. Knapper, N. Russell, A. Gilkes, et al., A randomised assessment of adding the kinase inhibitor lestaurtinib to 1st-line chemotherapy for FLT3-mutated AML, Blood 129 (2017) 1143–1154.
[6] M. Nakao, S. Yokota, T. Iwai, et al., Internal tandem duplication of the flt3 gene found in acute myeloid leukemia, Leukemia 10 (1996) 1911–1918.
[7] Y. Yamamoto, H. Kiyoi, Y. Nakano, et al., Activating mutation of D835 within the activation loop of FLT3 in human hematologic malignancies, Blood 97 (2001) 2434–2439.
[8] N. Daver, R.F. Schlenk, N.H. Russell, et al., Targeting FLT3 mutations in AML: review of current knowledge and evidence, Leukemia 33 (2019) 299–312.
[9] Q.Y. Lan, Y.L. Zhi, H. Heng, et al., Chemical space of FLT3 inhibitors as potential anti-AML drugs, Recent Pat. Anticancer Drug Discov. 12 (2017) 296–322.
[10] F. Ravandi, J.E. Cortes, D. Jones, et al., Phase I/II study of combination therapy with sorafenib, idarubicin, and cytarabine in younger patients with acute myeloid leukemia, J. Clin. Oncol. 28 (2010) 1856–1862.
[11] M. Levis, Midostaurin approved for FLT3-mutated AML, Blood 129 (2017) 3403–3406.
[12] A. Galanis, H. Ma, T. Rajkhowa, et al., Crenolanib is a potent inhibitor of FLT3 with activity against resistance-conferring point mutants, Blood 123 (2014) 94–100.
[13] P.P. Zarrinkar, R.N. Gunawardane, M.D. Cramer, et al., AC220 is a uniquely potent and selective inhibitor of FLT3 for the treatment of acute myeloid leukemia (AML), Blood 114 (2009) 2984–2992.
[14] L.Y. Lee, D. Hernandez, T. Rajkhowa, et al., Preclinical studies of gilteritinib, a next-generation FLT3 inhibitor, Blood 129 (2016) 257–260.
[15] O.Q. Yin, Y. Wang, H. Schran, A mechanism-based population pharmacokinetic model for characterizing time-dependent pharmacokinetics of midostaurin and its metabolites in human subjects, Clin. Pharmacokinet. 47 (2008) 807–816.
[16] I.K. Park, B. Mundy-Bosse, S.P. Whitman, et al., Receptor tyrosine kinase axl is required for resistance of leukemic cells to FLT3-targeted therapy in acute myeloid leukemia, Leukemia 29 (2015) 2382–2389.
[17] C.C. Smith, K. Lin, A. Stecula, et al., FLT3 D835 mutations confer differential resistance to type II FLT3 inhibitors, Leukemia 29 (2015) 2390–2392.
[18] C.C. Smith, Q. Wang, C.S. Chin, et al., Validation of ITD mutations in FLT3 as a therapeutic target in human acute myeloid leukemia, Nature 485 (2012) 260–263.
[19] X. Ren, X. Pan, Z. Zhang, et al., Identification of GZD824 as an orally bioavailable inhibitor that targets phosphorylated and nonphosphorylated breakpoint cluster region-Abelson (Bcr-Abl) kinase and overcomes clinically acquired mutation-induced resistance against imatinib, J. Med. Chem. 56 (2013) 879–894.
[20] Y. Wang, Y.L. Zhi, Q.M. Jin, et al., Discovery of 4-((7*H*-pyrrolo[2,3-d]pyrimidin-4-yl)amino)-*N*-(4-((4-methylpiperazin-1-yl)methyl)phenyl)-1*H*-pyrazole-3-carboxamide (FN-1501), an FLT3- and CDK-Kinase inhibitor with potentially high efficiency against acute myelocytic leukemia, J. Med. Chem. 61 (2018) 1499–1518.
[21] Y.L. Zhi, B.Q. Li, C. Yao, et al., Discovery of the selective and efficacious inhibitors of FLT3 mutations, Eur. J. Med. Chem. 155 (2018) 303–315.
[22] H. Heng, Y.L. Zhi, H.L. Yuan, et al., Discovery of a highly selective FLT3 inhibitor with specific proliferation inhibition against AML cells harboring FLT3-ITD mutation, Eur. J. Med. Chem. 163 (2019) 195–206.
[23] J. Ash, D. Fourches, Characterizing the chemical space of ERK2 kinase inhibitors using descriptors computed from molecular dynamics trajectories, J. Chem. Inf. Model. 57 (2017) 1286–1299.